

UNIVERSITY OF TARTU  
Institute of Computer Science  
Computer Science Curriculum

Mykhailo Nitsenko

Quantum circuit fusion in the presence of  
quantum noise on NISQ devices

Master Thesis (30 ECTS)

Supervisors: Dr. Dirk Oliver Theis (Ketita Labs OÜ)  
Prof. Dominique Unruh (University of Tartu)

Tartu 2020

## **Quantum circuit fusion in the presence of quantum noise on NISQ devices**

**Abstract:** Quantum computing is a rapidly developing field. Nevertheless, devices that are currently available and, most likely, will be available in the near future are noisy. This noise is the main barrier that does not allow humanity to efficiently perform quantum computations and achieve a stable general purpose quantum supremacy. This thesis project investigates a quantum fusion technique that can, potentially, sufficiently reduce statistical noise to reach the Heisenberg limit of quantum metrology. The proposal was implemented and experiments were performed using publicly available quantum computers of IBM Q. The experiments were conducted using variational quantum circuits in systems from 2 to 5 qubits and the exact copies of the experiments were performed on a simulator. Results were compared and studied using Fourier analysis.

**Keywords:** Quantum computer, NISQ devices, quantum noise, statistical noise, quantum circuit fusion, maximum likelihood estimation (MLE), Fourier analysis, IBM Quantum Experience, Qiskit, Amplitude Estimation, Grover operator.

**CERCS:** P170 Computer science, numerical analysis, systems, control

## **Kvantlülituse sulandumine kvantmüra olemasolul NISQ-seadmetes**

**Lühikokkuvõte:** Kvantarvutamine on kiiresti arenev valdkond. Sellele vaatamata on praegu ja tõenäoliselt ka lähitulevikus saadaval olevad seadmed mürarikkad. Müra on peamine barjäär, mis ei võimalda inimkonnal tõhusalt kvantarvutusi teha ja saavutada stabiilne üldotstarbeline kvantüleemus (quantum supremacy). Selles lõputöös uuritakse *quantum circuit fusion* tehnikat, mis võib potentsiaalselt piisavalt vähendada statistilist müra, et jõuda Heisenbergi piirini (Heisenberg limit of quantum metrology). Ettepanek viidi ellu ja katsed viidi läbi, kasutades IBM Q avalikult kättesaadavaid kvantarvuteid. Katsed viidi läbi 2 kuni 5 kvantbitiga variatsiooniliste kvantskeemide süsteemides. Katsete täpsed koopiad tehti simulaatoril. Tulemusi võrreldi ja uuriti Fourieri analüüsi abil.

**Võtmesõnad:** kvantarvuti, NISQ seadmed, kvantmüra, statistiline müra, *quantum circuit fusion*, maksimaalse tõenäosuse hinnang (MLE), Fourieri analüüs, IBM Quantum Experience, Qiskit, amplituudi hinnang, operaator Grover.

**CERCS:** P170 Arvutiteadus, arvutusmeetodid, süsteemid, juhtimine (automaatjuhtimisteooria)

## **Acknowledgement**

Author acknowledges the use of IBM Q for this work. The views expressed are those of the author and do not reflect the official policy or position of IBM or the IBM Q team.

The thesis research was conducted under the supervision of Ketita Labs OÜ. The views expressed are those of the author and do not reflect the official policy or position of Ketita Labs OÜ.

Quantum circuits were visualized using Qiskit (<https://qiskit.org>).

Plots were drawn using Matplotlib (<https://matplotlib.org>).

# Table of Contents

<b>1 Introduction</b>	<b>6</b>
<b>2 Methodology</b>	<b>8</b>
2.1 The quantum circuit fusion technique	8
2.2 Cloud quantum computing devices	9
2.3 Description of the quantum circuits	11
2.4 Tools and limitations	13
2.5 Analysis applied to the results	17
<b>3 Experiments and Results</b>	<b>19</b>
3.1 Expectation value function	19
3.1.1 Introduction and definitions	19
3.1.2 Experiments on 2 qubit systems	20
3.1.3 Experiments on 3 qubit systems	27
3.1.4 Experiments on 4 qubit systems	32
3.1.5 Experiments on 5 qubit systems	35
3.2 Quantum circuit fusion	37
3.2.1 Application to the simulations	39
3.2.1 Application to the 2 qubit circuit	43
3.2.2 Application to the 3 qubit circuit	47
3.2.3 Application to the 4 and 5 qubit circuits	50
<b>4 Conclusion</b>	<b>54</b>
<b>References</b>	<b>56</b>
<b>Appendix</b>	<b>59</b>
I. Figures and tables of the experiments excluded from section 3	59
<b>License</b>	<b>69</b>

# 1 Introduction

Near-term quantum computing is characterized by the scarcity of qubits and unavailability of quantum error correction. The term *Noisy Intermediate-Scale Quantum* (NISQ) computing has been coined by John Preskill [1] for this situation. Computing on NISQ devices suffers from two obstacles:

1. Quantum Noise: Quantum states that are prepared by running quantum circuits to yield useful information are subject to quantum error such as decoherence occurring during the runs of the circuits.
2. Statistical Noise: The impracticality of using complex quantum algorithms such as quantum amplitude estimation results in high variances of measurement output, requiring many shots (repeatedly preparing and measuring) for each circuit. The precision of estimating an observable through  $N$  measurements scales according to the shot-noise limit  $\frac{1}{\sqrt{N}}$ , while on a fault-tolerant quantum computer, the so-called quantum metrology limit  $\frac{1}{N}$  could be easily realized [2].

Typically, approaches to mitigate the statistical noise (2) increase the depth of the quantum circuits and hence make the quantum noise (1) worse.

Quantum Amplitude Estimation (QAE) [3] based on Quantum Phase Estimation (QPE) is a fundamental algorithm for quantum computing. Devices exhaustively described by the term NISQ [1] are already available to the public [4]. Nevertheless, the algorithm is too expensive for such devices and near-term quantum computing in general. There are proposals to "hybridize" the QPE algorithm - combine quantum computations with classical - to reduce the quantum cost or provide an alternative to it for a particular task [5], [6], [7], [8], [9], [10], [11].

This thesis project considers another approach of "hybridization" of the algorithm proposed by Suzuki et al. [12] to come close to the quantum metrology limit through a combination of amplitude amplification iteration ideas and maximum likelihood estimation. QAE has at its core the Grover iteration. The idea is to run a variable number  $m$  of Grover iterations, without auxiliary qubits or controlled operations, and make only a few shots to estimate the amplified probability  $p_m$ . Then use maximum likelihood to combine the results to obtain the final probability  $p$ .

The project aims to visualize and quantify the information loss incurred with increasing number of amplitude amplification iterations. The ansatz is to use Fourier analysis techniques for both the visualization and quantification.

To achieve the stated goals, software has been developed using Qiskit framework [13] for near-term quantum computing. The quantum fusion technique proposed by Suzuki et al. [12] was implemented. For the visualization and quantification of the information loss based on Fourier analysis the basic quantum circuit under consideration is parameterized by a real number  $t$ . The circuit prepares a parameterized quantum state  $|\psi_t\rangle$ , or, unintentionally, in the presence of decoherence, a mixed state  $\rho_t$ . The expectation value of measuring the Pauli-Z observable of an arbitrary qubit participating in the ideal error-free quantum state would describe a cosine function; adding amplitude amplification iterations give functions which can also easily be described.

The result of estimating the quantum circuit run on an error-prone quantum computing device have then been compared, visually by plotting the functions, as well as numerically using Fourier analysis techniques, to the true function. The number of qubits was chosen between 2 and 5, and the circuits were run on the `ibmq_5_yorktown` device [14] and `ibmq_qasm_simulator` quantum circuit simulator [15] publicly available via IBM Quantum Experience cloud platform [4].

The thesis consists of the three main sections:

1. Section 2 outlines the quantum fusion technique, details of the implementation used in this thesis, tools that were used and how the results were analysed;
2. Section 3 describes in depth experiments that were performed, discusses findings and proposes explanations of the results observed;
3. Section 4 summarizes the results of this work.

## 2 Methodology

This section describes in depth each logical part of the research that was assembled.

### 2.1 The quantum circuit fusion technique

The idea behind the technique is described and proven on the pages of “Amplitude Estimation without Phase Estimation” [12]. The core principles from the referenced paper will be outlined in this section.

Unitary operators  $A$ ,  $A^{-1}$ ,  $S_0$  and  $S_x$  that act on  $n$  qubit systems are defined as:

- $A|0\rangle_n = |\psi\rangle = \sqrt{a}|\psi_1\rangle|1\rangle + \sqrt{1-a}|\psi_0\rangle|0\rangle$ , where  $|\psi_1\rangle$  and  $|\psi_0\rangle$  are  $(n-1)$  qubit systems considered to be “good” and “bad” states respectively;
- $A^{-1}$  is the inverse of  $A$ , e.g.  $A^{-1}A = AA^{-1} = I$ ;
- $S_0$  is an operator that puts a negative sign to the all-zero computational basis state and does nothing to all orthogonal states, e.g.  $S_0|0\rangle_n = -|0\rangle_n$ ,  $S_0|\psi'\rangle = |\psi'\rangle$  for  $\forall |\psi'\rangle : |\psi'\rangle \perp |0\rangle_n$ ;
- $S_x$  is an operator that puts a negative sign to the “good” state and does nothing to the “bad” state, e.g.  $S_x|\psi_1\rangle|1\rangle = -|\psi_1\rangle|1\rangle$ ,  $S_x|\psi_0\rangle|0\rangle = |\psi_0\rangle|0\rangle$ .

Using these operators one can perform an amplitude amplification [16], [17] that is a generalization of Grover’s quantum search algorithm [18]. It allows to obtain “good” state with a higher probability by applying iteratively Grover operator:

$$Q = -AS_0A^{-1}S_x \quad (2.1)$$

to the state  $|\psi\rangle$  instead of performing measurements right away. It is shown by Brassard et al. in [19] that iterative application of  $Q$  to  $|\psi\rangle$  can be expressed as

$$Q^m|\psi\rangle = \sin((2m+1)\theta_a)|\psi_1\rangle|1\rangle + \cos((2m+1)\theta_a)|\psi_0\rangle|0\rangle \quad (2.2)$$

where parameter  $\theta_a$  is defined as  $\sin^2\theta_a = a$ ,  $m$  is the number of iterations  $|\psi_0\rangle$  and  $|\psi_1\rangle$  are quantum states. Suppose the state (2.2) was prepared  $N$  times, the rightmost qubit was measured and  $h$  times the value 1 was observed. The likelihood function can be constructed for this probabilistic event:

$$L(h; \theta_a) = [\sin^2((2m+1)\theta_a)]^h [\cos^2((2m+1)\theta_a)]^{N-h} \quad (2.3)$$

the binomial coefficient ( $N$  choose  $h$ ) is suppressed because it does not depend on the parameter  $\theta_a$ .

Consider a set of experiments  $m = (m_0, m_1, \dots, m_M)$  with  $N = (N_0, N_1, \dots, N_M)$  measurements and  $h = (h_0, h_1, \dots, h_M)$  good outcomes respectively, the combined likelihood function (2.3) can be expressed as:

$$L(h; \theta_a) = \prod_{k=0}^M L_k(h_k; \theta_a) = \prod_{k=0}^M [\sin^2((2m_k + 1)\theta_a)]^{h_k} [\cos^2((2m_k + 1)\theta_a)]^{N_k - h_k} \quad (2.4)$$

Given the likelihood function, maximum likelihood (ML) estimate can be expressed as:

$$\theta'_a = \operatorname{argmax}_{\theta_a} L(h; \theta_a) = \operatorname{argmax}_{\theta_a} \ln L(h; \theta_a) \quad (2.5)$$

The equation (2.5) allows to determine  $\theta'_a$ , thus, to determine  $a' = \sin^2 \theta'_a$ .

Based on calculating the Fisher information of this unbiased estimator, the work of Suzuki et al. [12] gives families of experiment designs for which they prove, based on the Cramer-Rao theorem, that the quantum metrology limit is reached asymptotically.

It is important to notice that the algorithm is meaningful only if  $M > 0$  and  $\exists k : m_k \neq 0$ . The algorithm is described in the paper by Suzuki et al. [12] as “the *quantum circuit fusion* technique that combines some quantum circuits to determine the target value uniquely, while some quantum advantage is guaranteed”.

## 2.2 Cloud quantum computing devices

This section describes quantum computers available for public use via IBM Quantum Experience platform [4].

At the time when the research is made there are several distinctive backends available:

1. `ibmq_16_melbourne` [20] - 15 qubits, “grid” layout;
2. `ibmq_rome` [21] - 5 qubits, “chain” layout;
3. `ibmq_london` [22], `ibmq_burlington` [23], `ibmq_essex` [24], `ibmq_ourense` [25] and `ibmq_vigo` [26] - 5 qubits, “T-shaped” layout;
4. `ibmq_5_yorktown` [14] - 5 qubits, “butterfly” layout;
5. `ibmq_armonk` [27] - 1 qubit;

6. `ibmq_qasm_simulator` [14] - up to 32 qubits simulation.

Physical layouts are depicted in Figure 2.1 - arrows represent connections between qubits where 2-qubit operations are allowed, colors represent relative noise - lighter color means less noise. However, it is important to mention that the noise colors represent different values on different devices, therefore colors from Figure 2.1 can not be used for comparison between different backends. The values that the colors represent are publicly available at IBM Quantum Experience platform [4] where the images were sourced.

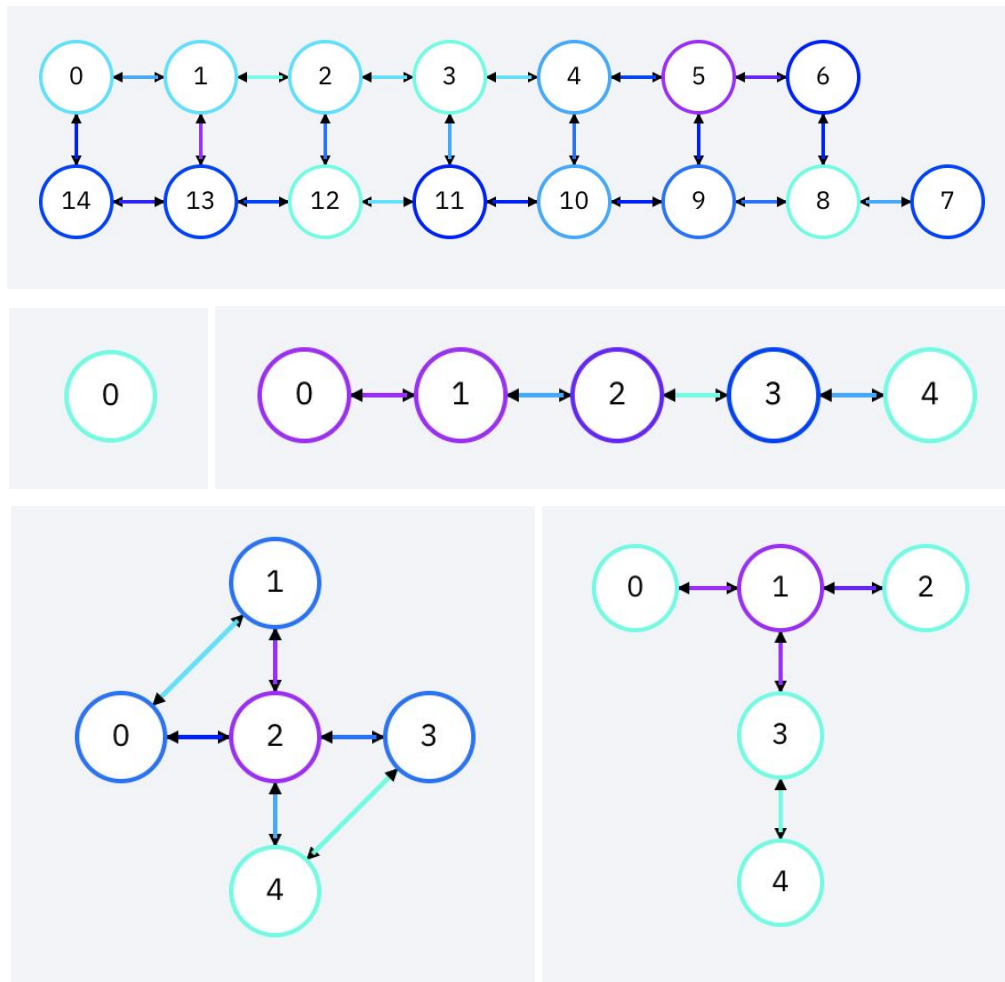


Fig. 2.1 Distinct physical layouts available via IBM Quantum Experience [4]. From top to bottom, left to right - `ibmq_16_melbourne` [20], `ibmq_armonk` [27], `ibmq_rome` [21], `ibmq_5_yorktown` [14] and `ibmq_london` [22].

`ibmq_5_yorktown` has sufficiently many qubits to perform experiments and observe quantum noise. The layout of the device allows it to have the most versatility in experiments. Therefore `ibmq_5_yorktown` was the main backend used to obtain results.

`ibmq_qasm_simulator` has the same API as real quantum devices - it allows users to reuse the codebase and perform the exact copy of experiments in a well-tuned environment.

The data returned from the simulator contain only statistical noise - an equivalent of a perfect quantum computer - it allows to compare results with the data returned from quantum computers to see the effect of quantum noise.

## 2.3 Description of the quantum circuits

In order to run quantum algorithms described in section 2.1 on a quantum computer, they need to be expressed in a sequence of primitive gates - a quantum circuit. This section describes how all the unitaries from the algorithm are defined.

First of all, the basic unitaries  $A$ ,  $A^{-1}$ ,  $S_0$  and  $S_x$  used in the algorithm are expressed as circuits of primitive discrete gates. The unitaries  $A^{-1}$  and  $S_x$  depend on the choice of  $A$  - the subject to which the quantum circuit fusion algorithm is applied.

Variational quantum circuits are a fundamental proposal for near-term quantum algorithms. Therefore, the following Hamiltonian simulation on  $j$  qubits was chosen to be the subject:

$$A_j = e^{-itX^{\otimes j}} \quad (2.6)$$

where  $t$  is a parameter,  $X^{\otimes j}$  is a sequence of tensors of Pauli-X gates  $j$  times, e.g  $X_3 = X \otimes X \otimes X$ . The unitary was translated into a circuit as described by Nielsen et al. [28] on page 210. An example of the 5 qubit circuit for the unitary  $A_5$  is depicted in Figure 2.2.

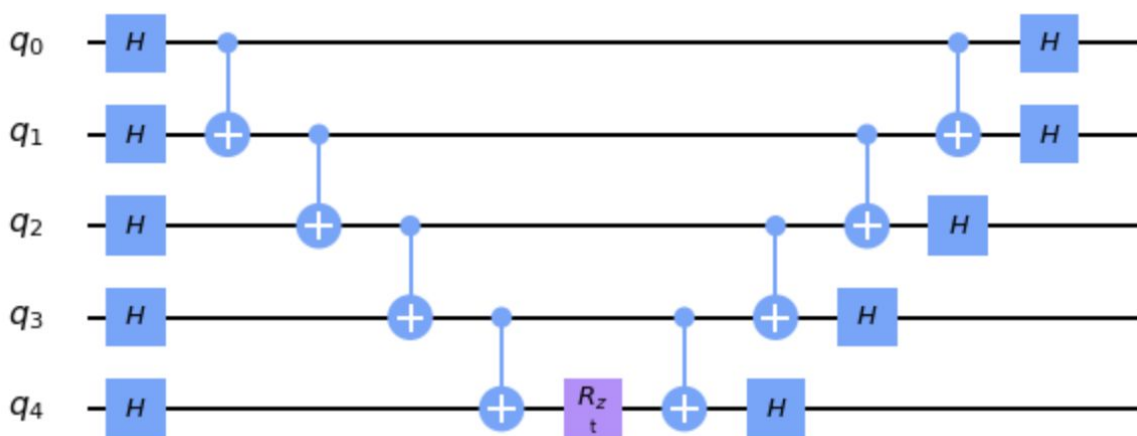


Fig. 2.2 A circuit for  $A_5$

This construction is simple enough to provide meaningful results even on NISQ devices that are currently available, nevertheless, it is complex enough to contain sufficient amount of

noise due to the abundance of CNOT gates. The unitary  $A^{-1}$  comes naturally from the expression (2.6):

$$A_j^{-1} = e^{itX^{2j}} \quad (2.7)$$

An example of the 5 qubit circuit for the unitary  $A_5^{-1}$  is depicted in Figure 2.3.

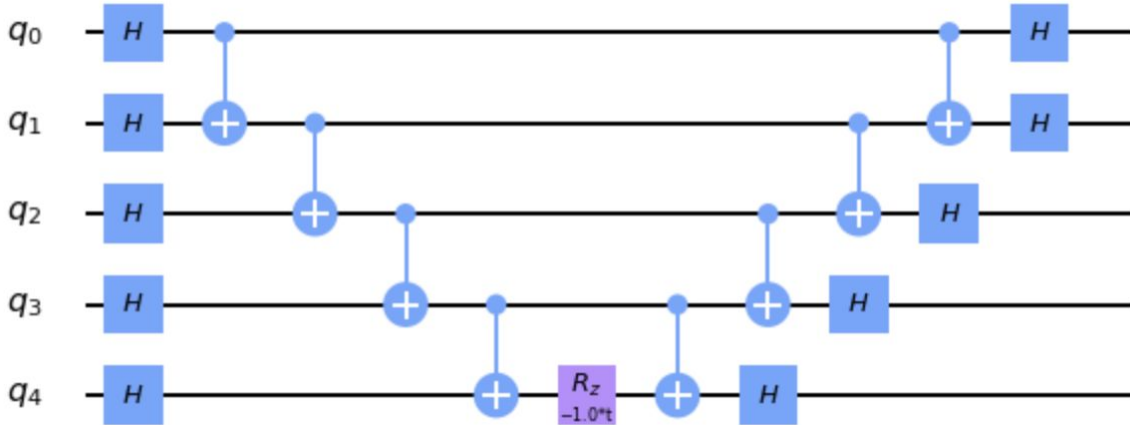


Fig. 2.3 A circuit for  $A_5^{-1}$

The unitary  $S_x$  was chosen to align with requirements of the algorithm - all the states that turns negative after  $S_x$  applications are considered “good” and all the other states are considered “bad”. The groups of “good” and “bad” states are needed only for evaluation of the algorithm performance, no other meanings of the results from the application of the algorithm to the Hamiltonian simulation  $A$  are discussed in the papers. Thus,  $S_x$  can be defined as  $S_{xj}$  that consists of Pauli-Z gate tensored with  $(j - 1)$  identity gates. For example,  $S_x$  for 5 qubit system can be written as  $S_{x5} = Z \otimes I \otimes I \otimes I \otimes I$ . The circuit for 5 qubit unitary  $S_x$  is depicted in Figure 2.4.

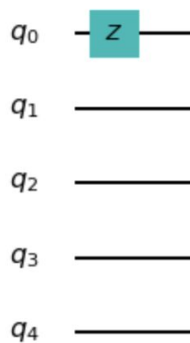


Fig. 2.4 A circuit for  $S_{x5}$

The last but not least is  $S_0$  - a unitary that puts a negative sign on the all zero state and does nothing to all the other states.

$$S_0 = I - 2|0\rangle_n \langle 0|_n \quad (2.8)$$

$S_0$  can be implemented in several ways depending on the number of qubits. For experiments in this paper the circuit construction was generalized in a construction algorithm. The steps of the algorithm to construct a circuit for  $S_0$  are the following:

1. Apply Pauli-X gates on all the qubits in the system;
2. Apply Hadamard gate on the qubit with index  $n - 1$  ;
3. Apply multi-controlled NOT gate with the controls on all the qubits except the target qubit with index  $n - 1$  ;
4. Applying Hadamard gate on the qubit with index  $n - 1$  ;
5. Apply Pauli-X gates on all the qubits in the system.

One can prove correctness of the construction by applying the obtained circuit to the computational basis states of the system. Examples of the circuits for 2 and 3 qubit systems are depicted in Figure 2.5.

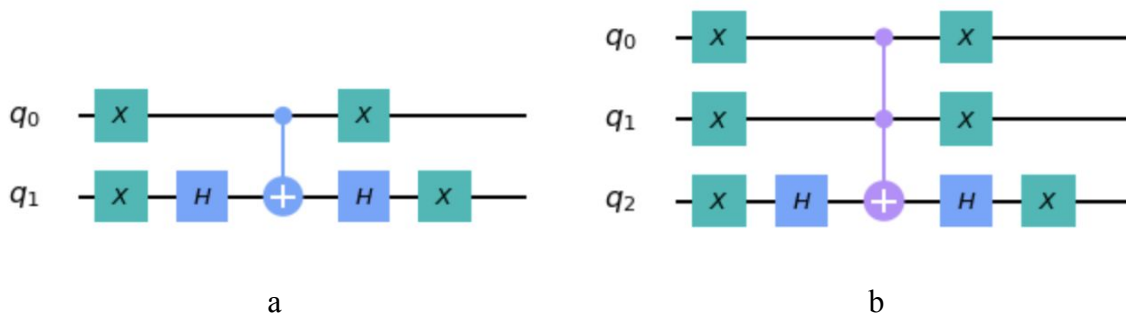


Fig. 2.5 Circuits for  $S_0$  for 2 qubit (a) and 3 qubit (b) systems

And finally, a circuit for unitary  $Q$  can be constructed as defined in the expression (2.1) - by appending circuits of the terms from right to left - the same way as they are applied in the algorithm to the state of the quantum system.

## 2.4 Tools and limitations

The quantum (circuits) and classical (ML estimation) parts of the algorithm were translated to a software that is capable of assembling experiments and processing results. This section describes the software implementation for the research.

IBM Quantum Experience [4] provides a circuit composer interface that is depicted in Figure 2.6. It is easy to start constructing experiments and observe metrics of the circuits composed in real time, however, it is tedious to construct large parametrized circuits required for the research.

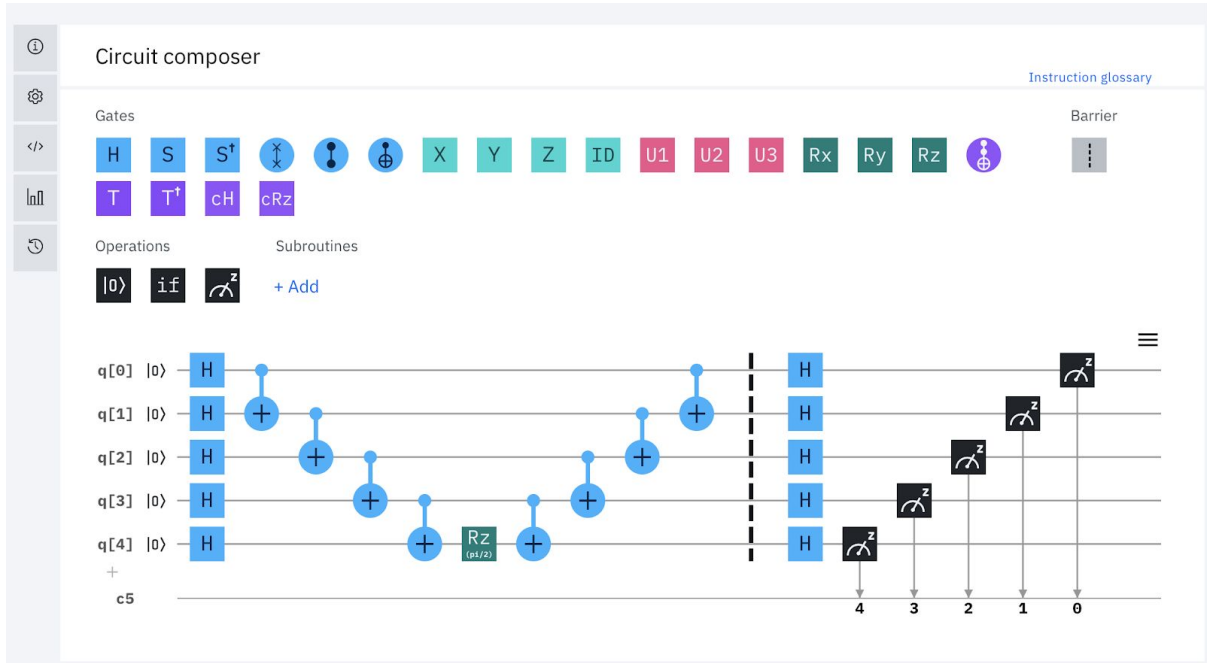


Fig. 2.6 IBM Quantum Experience [4] circuit composer interface

Therefore Qiskit [13] is used. Qiskit is a domain-specific language for programming quantum computing devices with Python [29]. It is an open source project under the leadership of IBM Corp. Qiskit allows constructing circuits and sending quantum circuits to backends via cloud API.

The circuit as seen in Figure 2.6 was composed using Qiskit in a Jupyter notebook [30] which is depicted in Figure 2.7. The software developed for this thesis project is not a standalone program but rather a set of utilities that were used to perform experiments and obtain results. The software - Python files and Jupyter notebooks - can be found in the public repository of the research [31].

```

In [1]: import math
        from qiskit import QuantumCircuit

        number_of_qubits = 5
        qc = QuantumCircuit(number_of_qubits, number_of_qubits)

        for i in range(number_of_qubits):
            qc.h(i)

        last_qubit_index = number_of_qubits - 1
        for i in range(last_qubit_index):
            qc.cx(i, i + 1)

        qc.rz(math.pi / 2, last_qubit_index)

        for i in reversed(range(last_qubit_index)):
            qc.cx(i, i + 1)

        qc.barrier()

        for i in range(number_of_qubits):
            qc.h(i)

        qc.measure([qbit for qbit in range(number_of_qubits)],
                   [cbit for cbit in range(number_of_qubits)])

        qc.draw(output="mpl")

```

Out[1]:

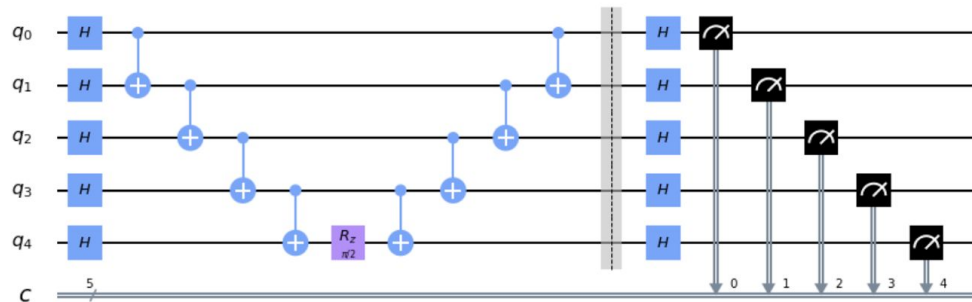
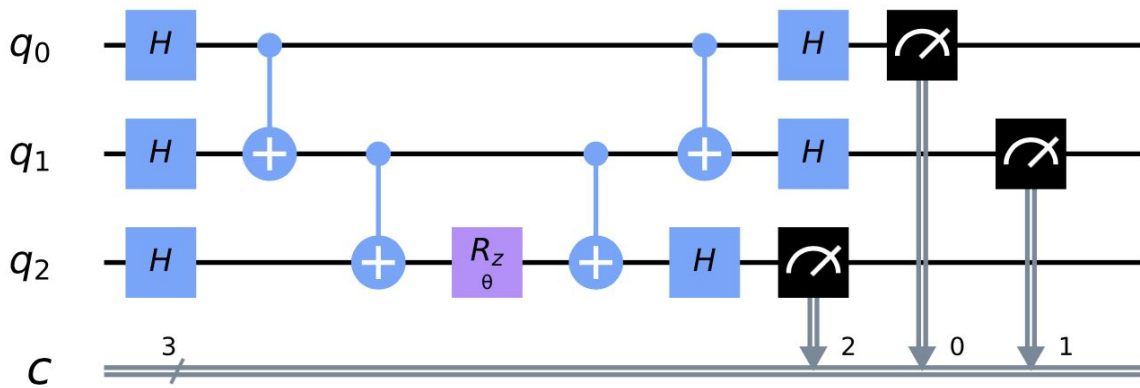
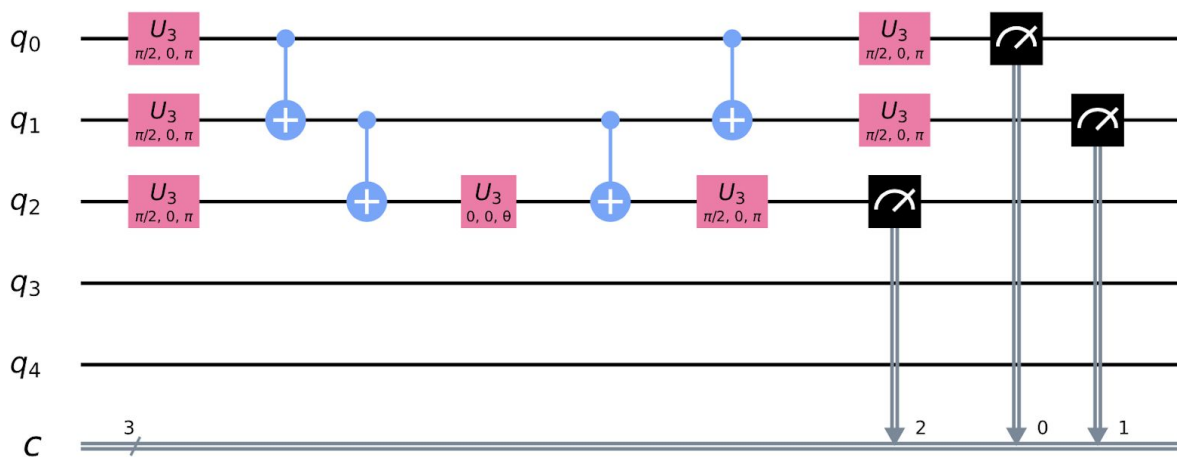


Fig. 2.7 An example of circuit composition using Qiskit in a Jupyter notebook

The tools developed contain, first of all, convenient wrappers that allow to streamline experiments. Circuits are composed using standard Qiskit APIs of circuit construction. Before being sent to a cloud backend, quantum circuits get optimized and converted from a set of conventional quantum logical gates into generalized U1, U2, U3 and CNOT gates for a particular backend that is provided as a parameter. These generalized gates are translated to pulses that interact with physical qubits on the device. It is important to be aware of the backend layout. Not all the circuits can be run on a physical quantum computer due to the lack of qubits or the lack of connections between them that allows for 2-qubits operations to be performed. Examples of a transpiled circuit can be seen in Figure 2.8.



a



b

Fig. 2.8 A quantum circuit with conventional quantum logical gates (a) and the same circuit transpiled for `ibmq_rome` (b)

Qiskit provides parameters that can be tuned to control transpilation procedure - optimization level and mapping of logical qubits to physical qubits are among these parameters. For this thesis parameters were kept to defaults. Picking the best parameters for the task is out of scope of this research and can be studied as a separate topic.

The number of experiments that can be performed are restricted with credits. The latest rule applied to an account at IBM Quantum Experience is 15 credits that are deduced when an experiment is submitted and returned when the experiment is completed. Each experiment that was performed for this thesis took 3 credits that means 5 experiments can be submitted at once. Depending on the level of business of the backend, each experiment took from 15 minutes to a couple of hours before results became available. Qiskit allows combining variational quantum circuits with different parameter values into one object via *parameter binding*. This combined object is treated as one experiment and was charged 3 credits as well. `ibmq_5_yorktown` allows up to 75 parameter values to be binded at once. Therefore, the

range of periodicity of the parameter  $t$  from the expression (2.6) was split into 75 evenly spaced values in range  $[0; 2\pi)$  and experiments were performed on these discrete values. For plotting, interpolation is used.

All the experiments are recorded in JSON format that contains id of an experiment, timestamp, information about the backend used for the experiment, parameters and binded values, comments and other information required to retrieve and analyse results later when the experiment is finished. After first retrieval, results are also recorded to the JSON file of the experiment in order to work with the results more efficiently in a long perspective.

The only way to obtain results from a quantum computer is to give a circuit enough shots to construct meaningful statistics to reason about the probability of the system to be in some particular state after application of the operator encoded in the circuit. IBM Q allows to choose from a set of predefined number of shots, at the time when the thesis is written 4 options are available - 1, 1024, 4096 and 8192 shots. Results are provided in a form of a dictionary where keys are strings of bits (e.g. "101010") and values are integers. All the integer values sum up to the number of shots performed. Each key of the dictionary represents an observed value after application of  $Z$  measurements on each qubit of the quantum system and the value stored by this key represents how many times this outcome was observed among all shots. When interpreting results, it is important to know that logical qubit 0 in a circuit is the least significant bit in the string of bits and logical qubit with the biggest index (e.g. 4 for `ibm_5_yorktown`) is the most significant bit in the bitstring.

## 2.5 Analysis applied to the results

The data returned from quantum devices were interpreted and compared with those from a simulator that allows reasoning about the outcomes of the experiments. This section will describe methods that were used to analyze information obtained from quantum computers.

The variational quantum circuit is run several times for each parameter setting  $t = \frac{2\pi}{75} i$ , where  $i$  is an integer in range  $[0; 75)$ . For each  $t$ , the results of the shots are averaged to give an estimate of the expectation value as follows:

$$E_t = \frac{1}{N} \sum_{i=0}^{N-1} s_i(t) \quad (2.9)$$

where  $t$  is a parameter in the variational circuit,  $N$  is the number of shots of the circuit execution with the parameter  $t$  and  $s_i(t)$  is the result obtained from measuring the  $Z_0$  observable, i.e., +1, if measurement in the computational basis of qubit 0 resulted in  $|0\rangle$ , and -1 if it resulted in  $|1\rangle$ .

The resulting estimated expectation value function is compared to the theoretically "correct" expectation value function both visually (by plotting the functions) and analytically, by comparing Fourier amplitudes or curve-fitting parameters. This allows to detect, heuristically, the loss of information through noise (statistical noise and quantum noise).

Statistical noise and quantum noise change the function. They can:

- add higher frequencies, throw the actual frequencies off a little (that also changes the period) or both;
- change the amplitudes;
- change the phases.

To quantify noise in this work changes in amplitude, phase, frequency were allowed, but keep the set of frequencies fixed to  $\{0,1\}$ . The function of that type was fitted to represent the estimated expectation values returned from the quantum device the best. The parameters obtained from fitting allows the research to quantify the noise. To visualize noise, both functions - the noisy one and the correct one - are plotted with frequencies for comparison.

## 3 Experiments and Results

The section describes in depth the experiments that were performed and results that were observed. All the data used for plots in this section can be found in Appendix I.

### 3.1 Expectation value function

This section presents and discuss expectation value functions of  $Z_0$  observable for each experiment performed using the circuits defined in section 2.3. The numbers in this section are rounded to 5 digits after coma, such precision is representative enough to interpret results.

#### 3.1.1 Introduction and definitions

Experiments were performed using *ibmq\_5\_yorktown* and *ibmq\_qasm\_simulator* cloud backends that are publicly available via IBM Quantum Experience [4]. Results from the real quantum device and the simulator were obtained using 8192 shots for each point - each variational circuit with fixed parameters. It is the maximum number of shots allowed by IBM Q at the time. The circuits in the experiments are parameterized with  $t = [0; 2\pi)$ ,  $q = \{2, 3, 4, 5\}$  and  $m = \{0, 1, 2, 3, 4\}$ , where  $t$  is the parameter of the variational circuit,  $q$  is the number of qubits the circuit is using and  $m$  is the number of Grover iterations - exactly the  $m$  from the expression (2.2). Each set of  $(q; m)$  defines a separate experiment. Each such experiment was run using 75 evenly spaced values of  $t$  due to limitations discussed in section 2.4. For simplicity, experiments are referenced by the combination  $(q; m)$  (e.g. *experiment (2;0)*). Combination  $(q; m; t)$  defines a circuit of the experiment on which shots were performed, because all the parameters of variational circuits must be binded before execution as discussed in section 2.4, thus variational circuits with a fixed set of 75 parameter values become 75 different circuits that are not “variational” anymore.

The following function can easily be seen by elementary calculations to be the expectation value function of the  $Z_0$  observable for  $m = 0$ :

$$f(t) = \cos(t) \tag{3.1}$$

where  $t$  is the variational circuit parameter. The function (3.1) was parameterized as seen in the expression (3.2) in order to perform parameters fitting using results obtained during experiments:

$$f_p(t) = p_2 \cos(p_0 t + p_1) + p_3 \quad (3.2)$$

where  $p_0$ ,  $p_1$ ,  $p_2$  and  $p_3$  are parameters that are responsible for frequency, phase, amplitude and vertical shift of the function respectively and are used to quantify the effect of noise. Table 3.1 shows the values of parameters when all the noise - statistical and quantum - is absent, therefore the function (3.2) with parameters from Table 3.1 is exactly the candidate (3.1) that is further referenced as “the ideal function”.

Table 3.1 The “ideal” parameters of the observed expectation value function

$p_0$	$p_1$	$p_2$	$p_3$
1	0	1	0

In comparison, parameter values were fitted using  $t$  and  $f(t)$  values obtained from simulations and can be seen in Table 3.2. Mean square error (MSE) is calculated between values of the ideal function (3.1) and the function (3.2) with the parameters from the table to quantify how closely the ideal function is capable of representing the function observed in simulations.

Table 3.2 Parameters of the candidate for the expectation value function observed during experiments fitted using simulation results

$p_0$	$p_1$	$p_2$	$p_3$	MSE
0.99949	0.00373	0.99910	-0.00020	0.00005

It can be seen from Table 3.2 that the ideal function represents simulations - experiments in the presence of statistical noise only - sufficiently well, therefore the ideal function (3.1) is further referenced as “the true expectation value function” or “true function” for simplicity and simulations are used as a baseline for the further analysis.

### 3.1.2 Experiments on 2 qubit systems

This section describes different circuits executed and results obtained using 2 qubits with default layout from *ibmq\_5\_yorktown* backend.

Expectation values of  $Z_0$  observable from experiment (2;0) can be seen in Figure 3.1.

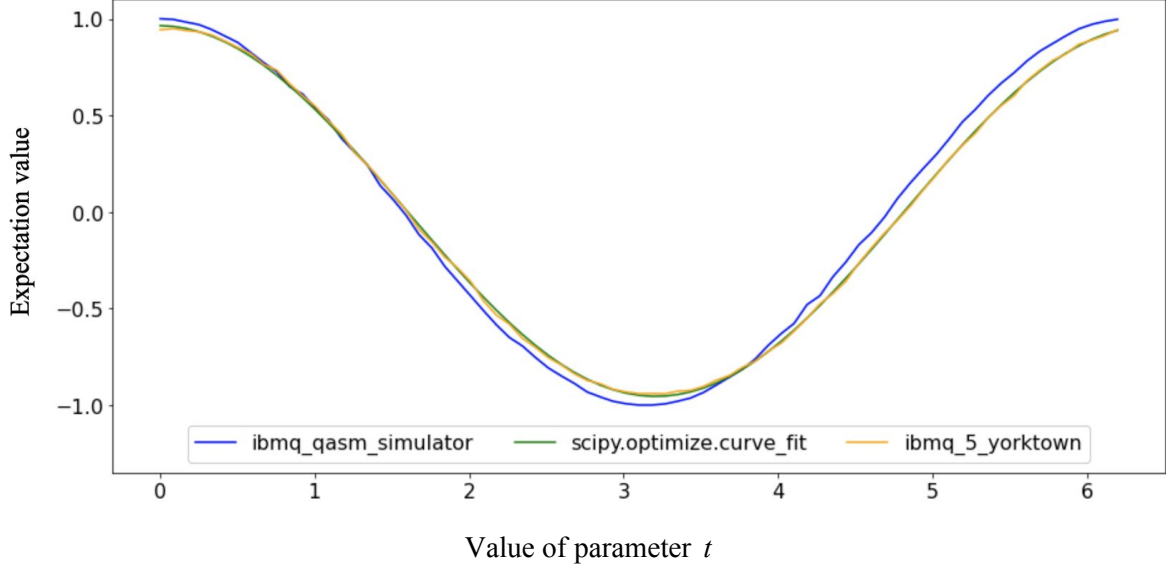


Fig. 3.1 Expectation values of experiment (2;0)

For each experiment defined by the combination  $(q; m)$  defined in the section 3.1.1 results here and further are compared in the same manner as seen in Figure 3.1. Expectation values are calculated from shots on a real quantum device and are compared visually side by side with the expectation values calculated from shots on a simulation. Experiments performed on the real quantum device are further referenced as “real experiments” and their counterparts performed using the simulator are referenced as “simulations”. It was shown that the function (3.2) fitted to a simulation results gains parameter values close to the true expectation value function. It is also known that simulations lack quantum noise and contain only statistical noise. Statistical noise does not allow parameters of simulation experiments to reach exact values of parameters of the true function. In the same way, one can observe and quantify quantum noise by fitting unknown parameters of the function (3.2) using real experiment values that contain both quantum and statistical noise. These fitted parameters in comparison with the parameters obtained from a simulation reveal the effect of quantum noise. The function (3.2) with the fitted parameters is plotted by the name of the fitting function used - *scipy.optimize.curve\_fit*. The function was used with default parameters. The fitted function plotted side by side with the real function allows one to see how closely the fitting procedure was capable of representing the values observed during the experiment on the quantum device.

From the visual comparison that Figure 3.1 provides it is visible that the *ibmq\_qasm\_simulator* curve mostly lies to the left from the *ibmq\_5\_yorktown* curve. It means that with the same parameter  $t$  in the variational circuit similar expectation values are observed earlier during the simulation than during the experiment on a quantum device. The observation is confirmed by the curve fitting procedure. The fitted parameters for the function (3.2) used to plot the *scipy.optimize.curve\_fit* curve can be seen in Table 3.3.

Table 3.3 Parameters of the expectation value function (3.1) fitted using results of the experiment (2;0) on *ibmq\_5\_yorktown*

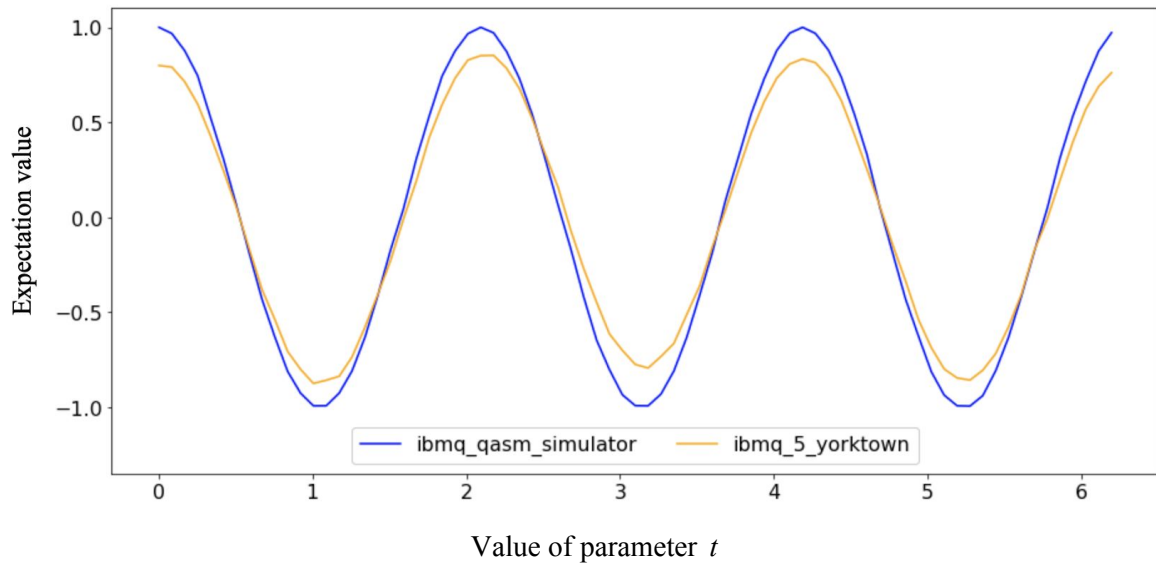
$p_0$	$p_1$	$p_2$	$p_3$	MSE
0.97453	0.01415	0.95939	0.00542	0.00011

The most prominent parameters are  $p_1$  and  $p_2$  that show the quantity of deviation from the true function in phase and amplitude respectively. These differences were visually observed in Figure 3.1.

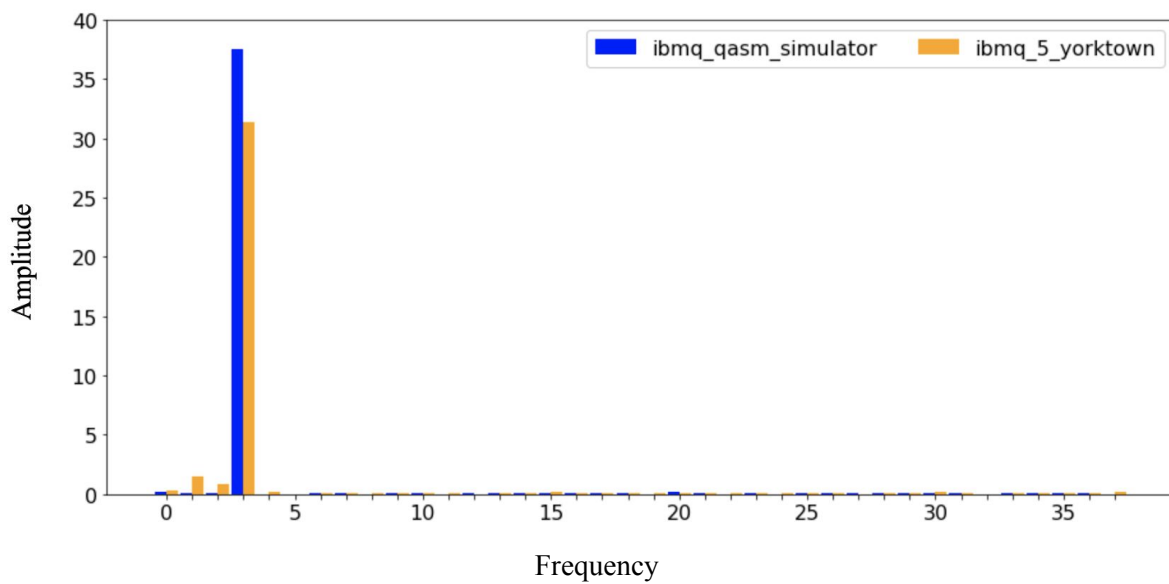
Quantum computers available publicly via IBM Quantum Experience are controlled by microwave pulses to rotate qubits towards ground and excited states that are interpreted as  $|0\rangle$  and  $|1\rangle$ . Specifications [32] from page 29 describes how OpenPulse can be used to perform experiments on a general quantum computer beyond OpenQASM capabilities. Qiskit textbook [33] in the section “6. Investigating Quantum Hardware Using Microwave Pulses” describes how qubits can be calibrated and how higher energy states can be accessed. Thus, difference in phase can be interpreted as imprecision of these pulses used to control qubits and amplitude differences are supposedly related to decoherence that the qubit system is a subject to.

It is also seen in Table 3.3 that the mean square error has grown twice as big compared to the fitted function of the simulation. As seen in Figure 3.1, the fitted curve is tightly aligned with the results of the *ibmq\_5\_yorktown* experiment. Therefore, it indicates that the *ibmq\_5\_yorktown* curve is not as smooth as the *ibmq\_qasm\_simulator* curve.

The next step is to observe how the 2 qubit system behaves in the presence of different iterations of Grover operator applications. Expectation values for experiments (2;1), (2;2), (2;3) and (2;4) can be seen in Figure 3.2, Figure 3.3, Figure 3.4 and Figure 3.5 respectively together with Fourier analysis since parameters fitting of the higher frequencies is a tedious task to perform.



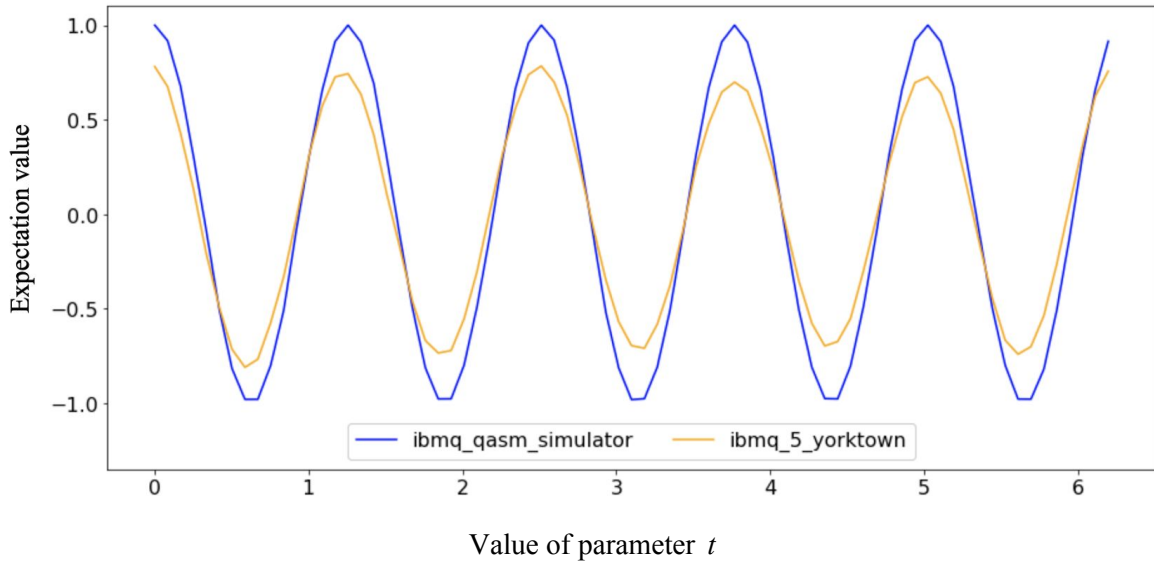
a



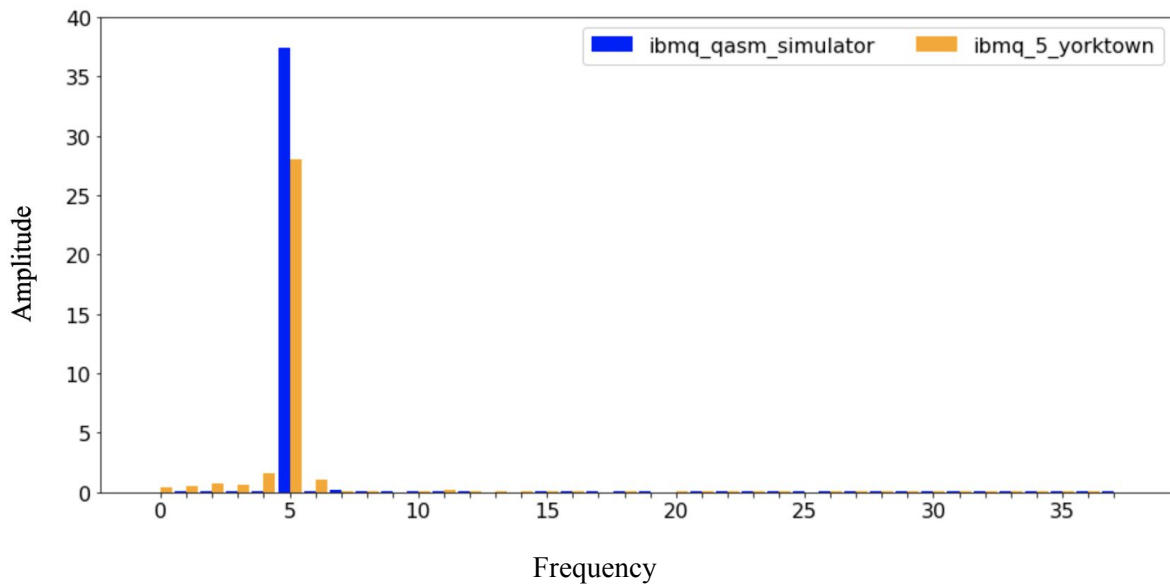
b

Fig. 3.2 Expectation values (a) and Fourier analysis (b) of experiment (2;1)

After the first iteration a similar picture can be seen in Figure 3.2 - the curve from the real quantum device is smaller in amplitude and shifted to the right slightly compared to the curve from a simulator. Fourier analysis allows us to see the presence of frequencies in the real experiment that are not present as much in the simulation. Both experiments contain statistical noise, therefore new frequencies can be the quantum noise that is present only in the real experiment. Comparable difference in the amplitudes of the dominant frequency is also visible in the analysis.



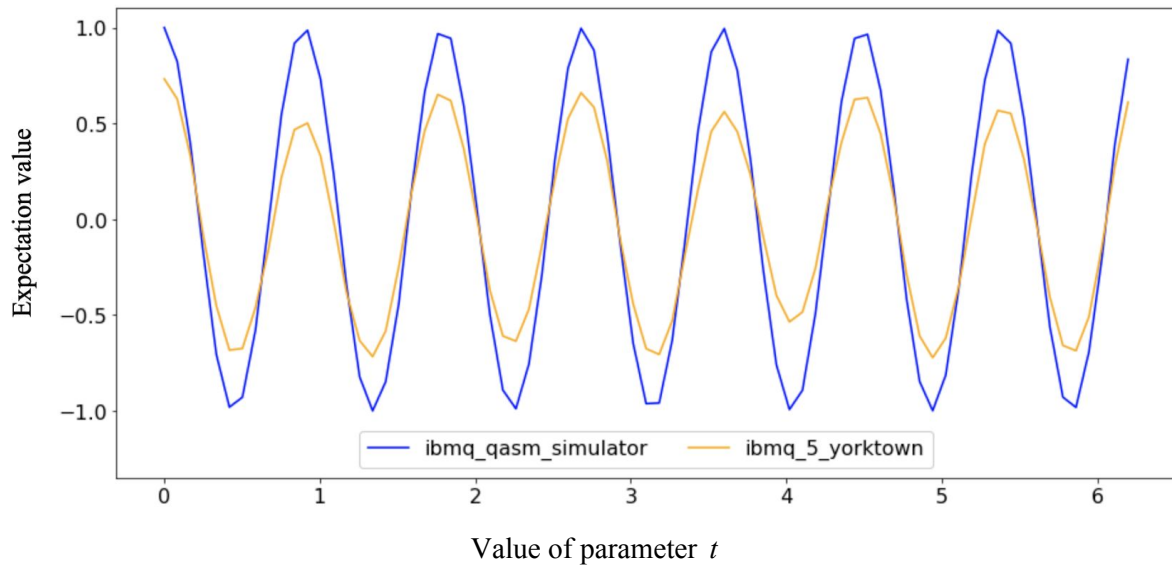
a



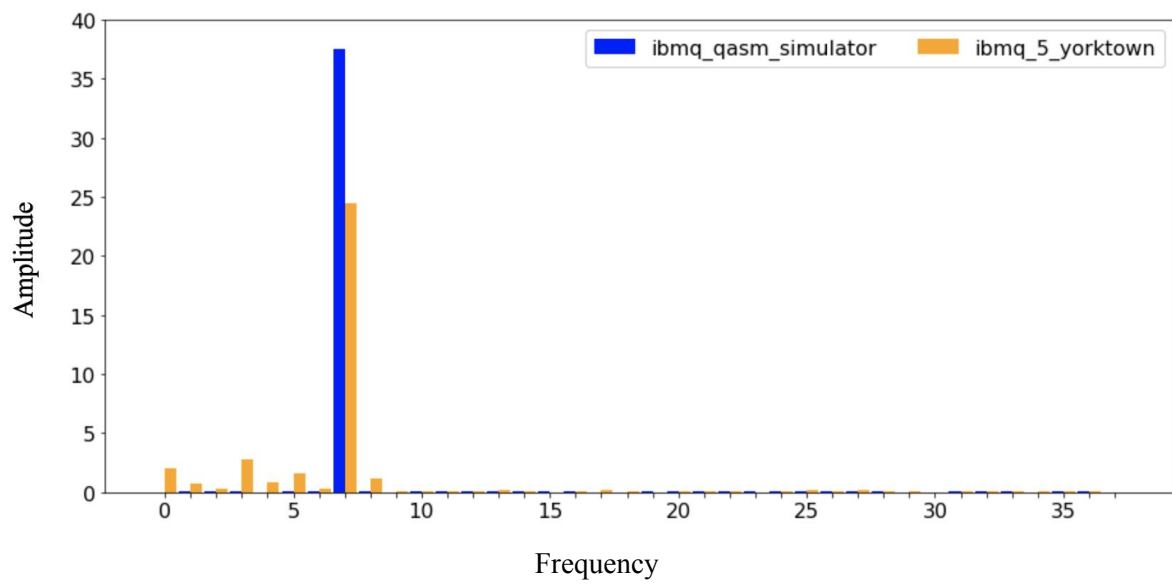
b

Fig. 3.3 Expectation values (a) and Fourier analysis (b) of experiment (2;2)

After two iterations it is visible in Figure 3.3 that the frequency drop continues and a slight shift to left now can be observed. The depth of the circuit without iterations used for experiment (2;0) is 6, the depth of the circuit with 1 iteration for experiment (2;1) is 16 and the depth for the circuit with 2 iterations for experiment (2;2) is 26. The values were obtained from the *depth* function of the *QuantumCircuit* object defined in Qiskit. Given a longer circuit, the program execution is longer. Given more time and gates, qubits are more exposed to the effect of decoherence. Supposedly, decoherence is the cause of the amplitude decrease of the expectation values from the experiments with more iterations.



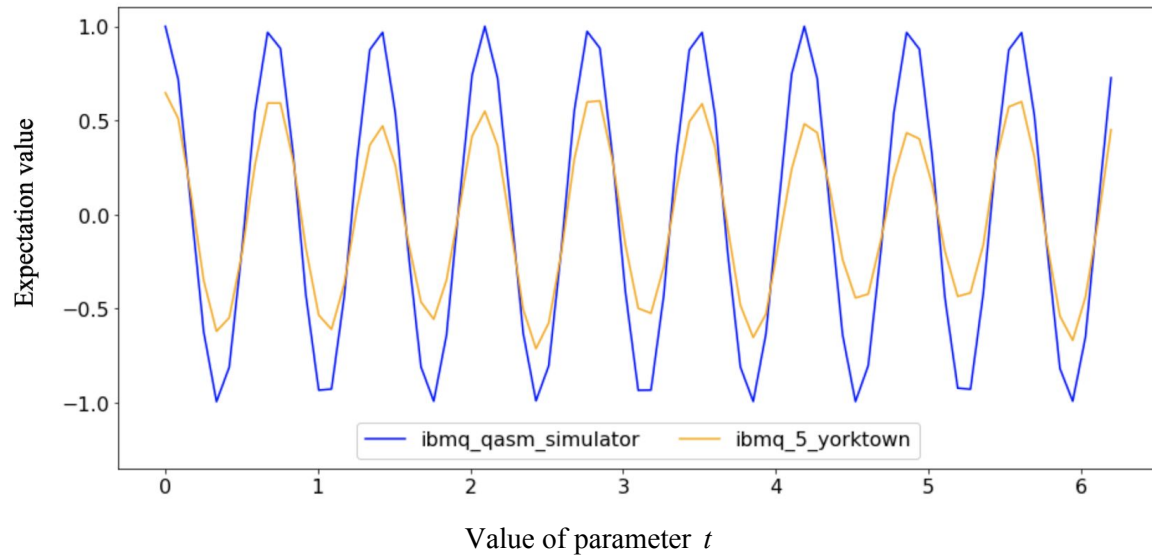
a



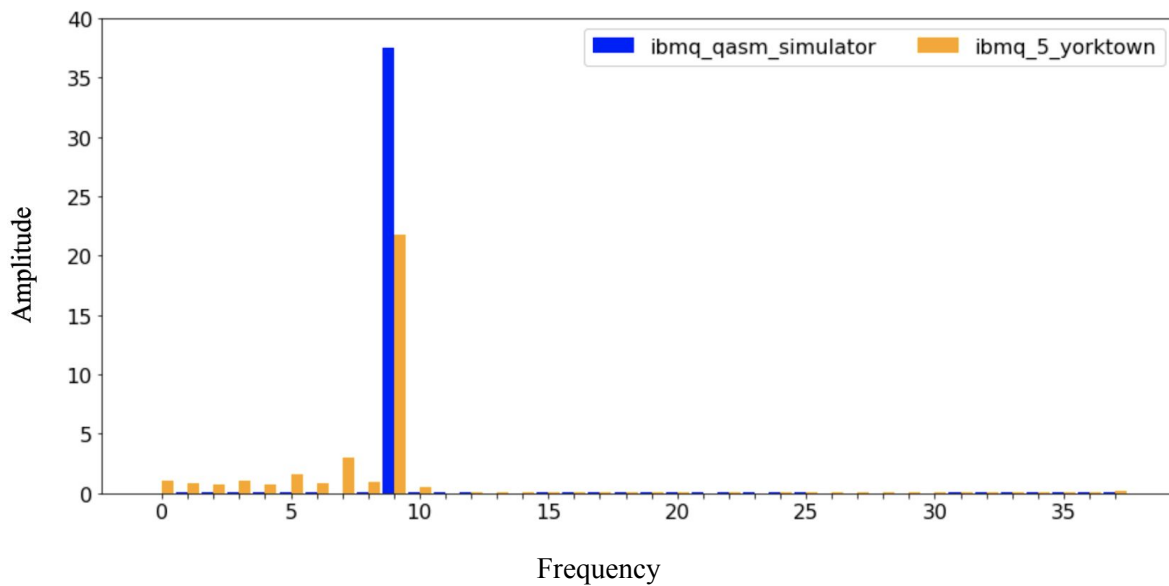
b

Fig. 3.4 Expectation values (a) and Fourier analysis (b) of experiment (2;3)

After three iterations additional frequencies seen in Figure 3.4 are the strongest so far. The amplitude decrease continues. The circuit depth for this experiment is 36 - steadily growing since each iteration adds 10 gates in total.



a



b

Fig. 3.5 Expectation values (a) and Fourier analysis (b) of experiment (2;4)

And last but not least, 4 iterations continues behavioural patterns of the previous experiments. The depth of the circuit is 46. It is visible how the number of points becomes almost not enough to represent the function efficiently. It is worth mentioning that these experiments are the best noise-wise because of the lowest circuit depth and the lowest number of qubits needed for the experiment. Circuit depth, as was discussed previously in this section, affects execution time, thus, potentially affects stability of the quantum system that is a subject to decoherence. The number of qubits used not only affects the circuit depth explicitly, but also, potentially, affects the amount of gate errors that may accumulate during execution.

### 3.1.3 Experiments on 3 qubit systems

This section describes different circuits executed and results obtained using 3 qubits with default layout from *ibmq\_5\_yorktown* backend.

Expectation values of  $Z_0$  observables from experiment (3;0) can be seen in Figure 3.1 and Table 3.4 describes values obtained by fitting parameterized function (3.2) using the expectation values of the real experiment.

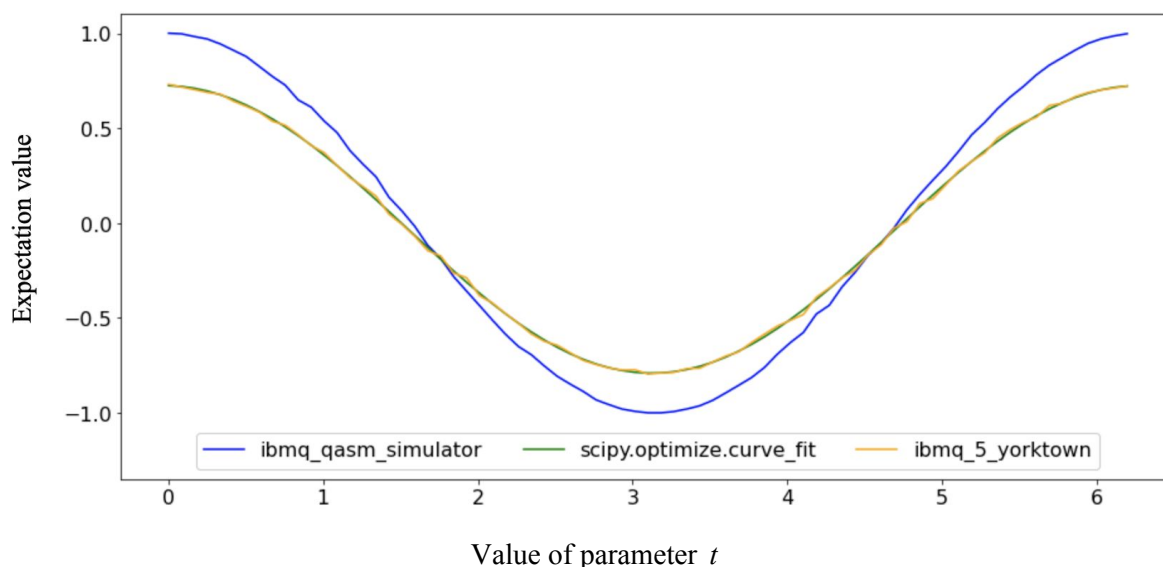
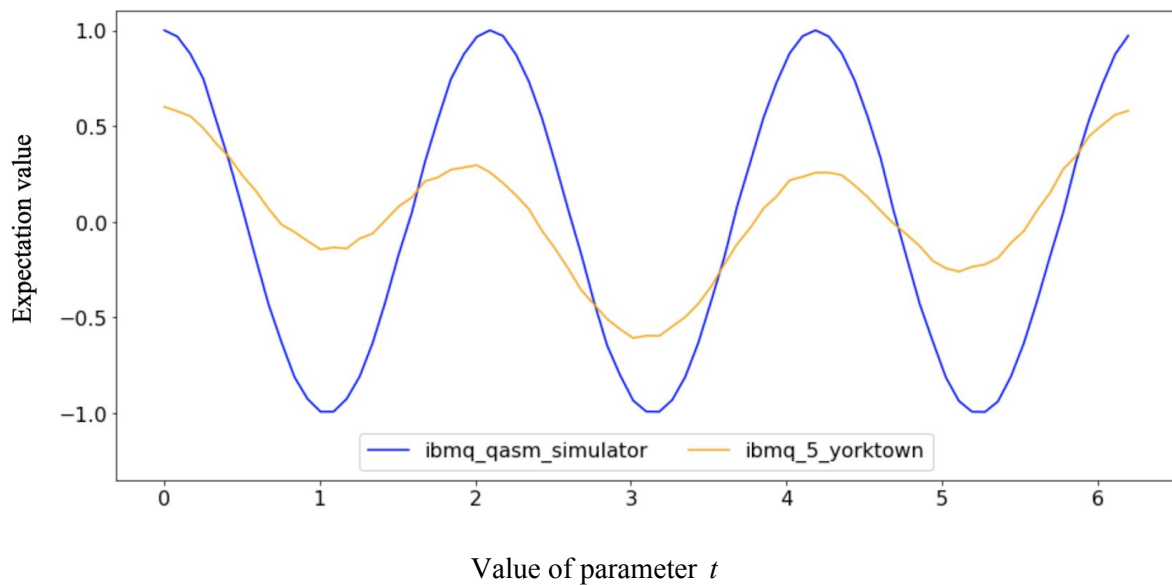


Fig. 3.6 Expectation values of experiment (3;0)

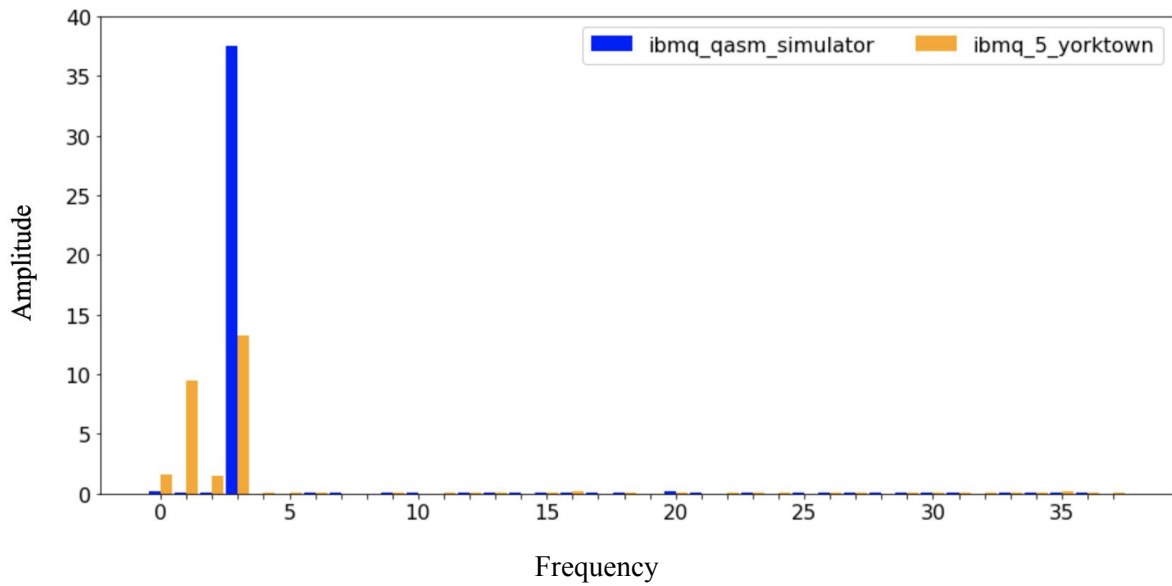
The circuit depth of the experiment grew naturally to 8 compared to experiment (2;0) to accommodate for an additional qubit. Parameters in Table 3.4 shows the visible amplitude difference between simulation and the real experiment. Also, a difference in phase and vertical shift that is not so obvious in Figure 3.6 is also quantified in Table 3.4. Experiments with different iterations applied are depicted in Figures 3.7-3.10.

Table 3.4 Parameters of the expectation value function (3.1) fitted using results of the experiment (3;0) on *ibmq\_5\_yorktown*

$p_0$	$p_1$	$p_2$	$p_3$	MSE
0.99726	0.02559	0.75740	-0.03312	0.00010



a

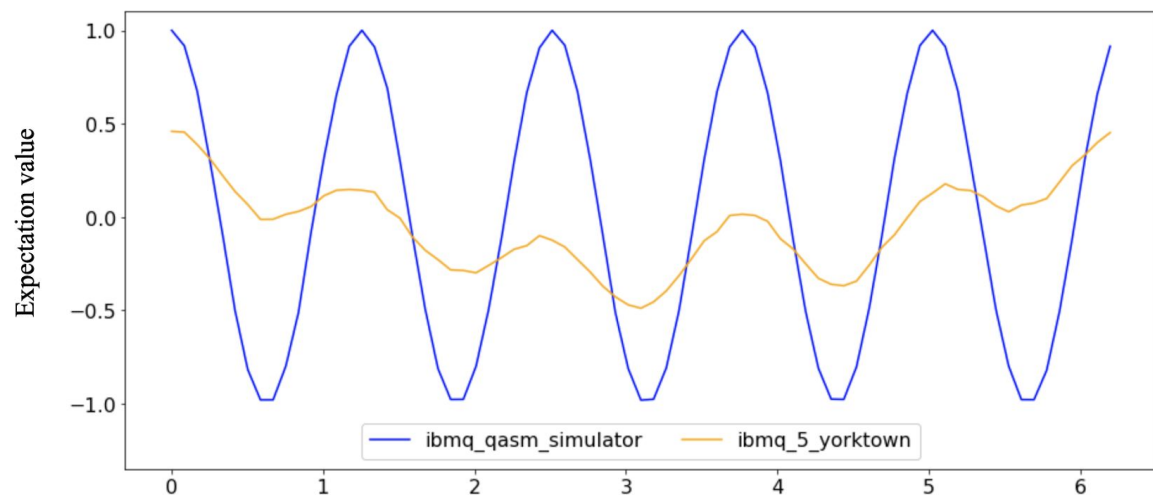


b

Fig. 3.7 Expectation values (a) and Fourier analysis (b) of experiment (3;1)

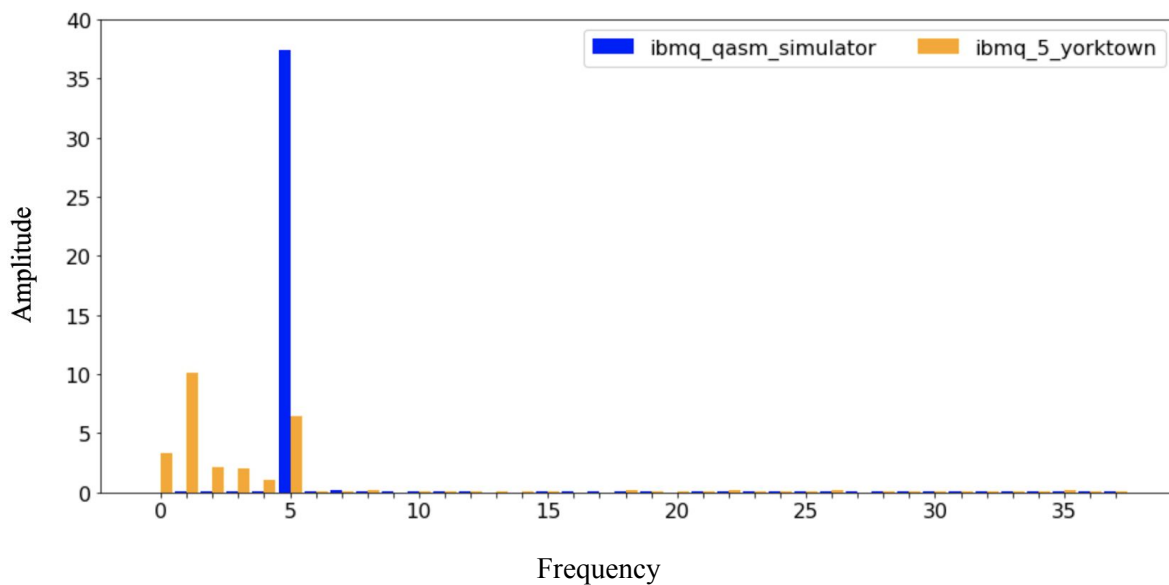
Other than the difference in depth, substantial difference in the 3 qubit circuits with iterations compared to the 2 qubit circuits with iterations is in the implementation of multi-controlled qubit gate that is used for the circuit of the operator  $S_0$ . 2 qubit systems use a simple CNOT gate to implement multi-controlled Pauli-X gate used in the circuit, while 3 qubit systems require a more complex CCNOT (Toffoli) gate that contains 6 CNOT gates and several single qubit gates in between. Thus, the circuit depth for experiment (3;1) is 31 gates even with a single application of Grover operator.

The amplitude decrease and the small shift to the right is also noticeable in the expectation values of the real experiment in comparison with a simulation depicted in Figure 3.7 (a) similarly to the 2 qubit system experiments. However, the most surprising is the curvature of the expectation values. Fourier analysis seen in Figure 3.7 (b) shows the presence of the strong lower frequencies that are absent in the simulation. Experiment (3;1) was recalculated and performed several times to confirm that there were no mistakes in the tools used. Nevertheless, similar pictures were obtained every time. Moreover, the trend continues throughout all the 3 qubit system experiments where the Grover operator is applied as seen in Figures 3.8 - 3.10.



Value of parameter  $t$

a

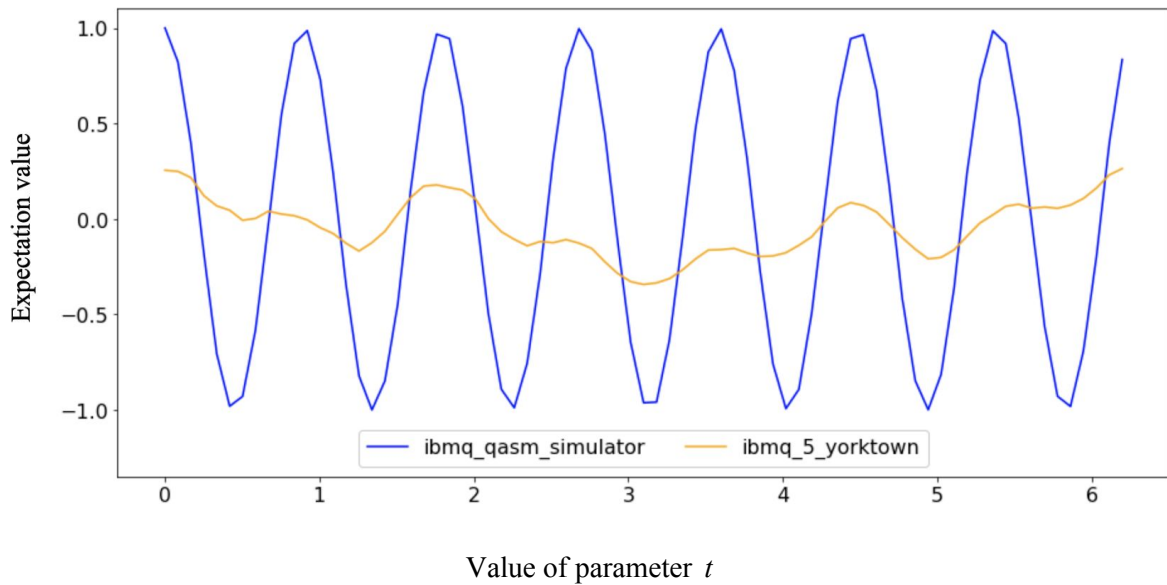


Frequency

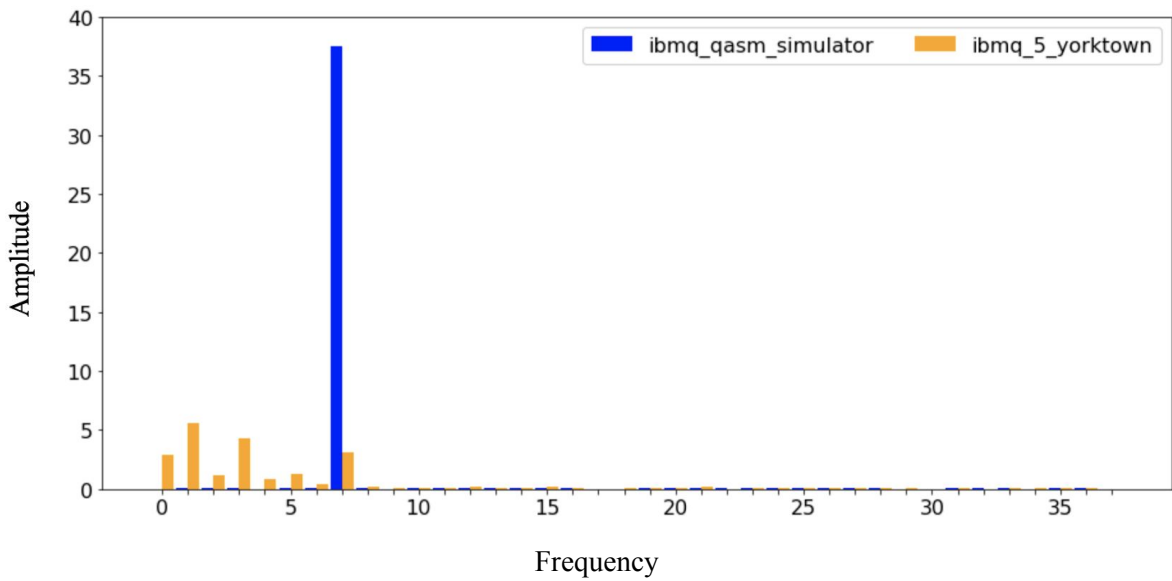
b

Fig. 3.8 Expectation values (a) and Fourier analysis (b) of experiment (3;2)

In fact, the first frequency becomes the dominant frequency in experiment (3;2) and not the expected fifth frequency observed in the simulation. The circuit depth of the experiment is 54.



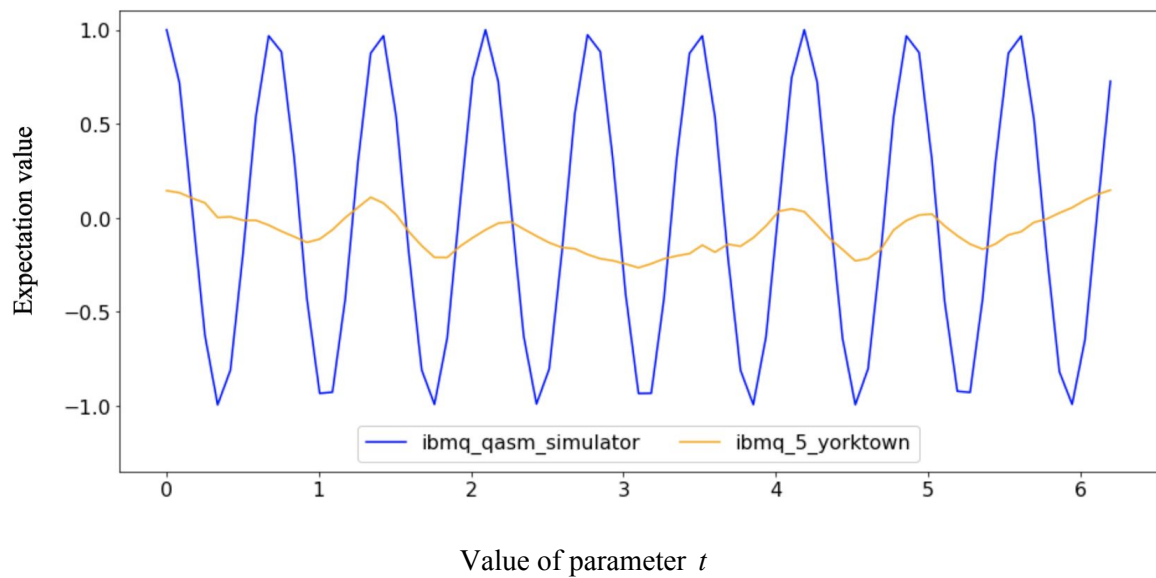
a



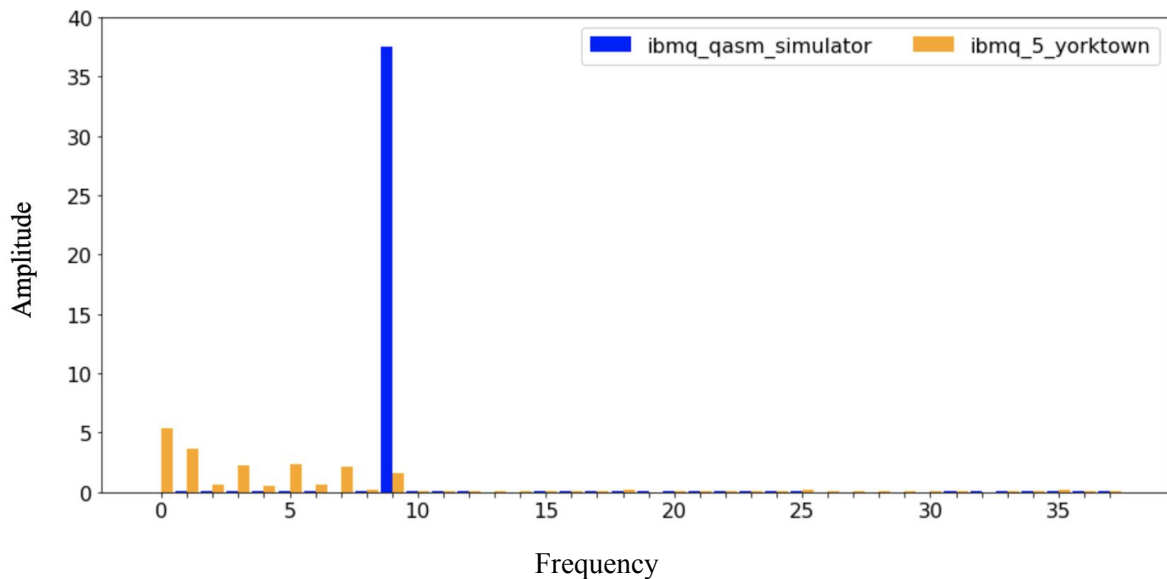
b

Fig. 3.9 Expectation values (a) and Fourier analysis (b) of experiment (3;3)

Experiment (3;3) continues trends of the severe amplitude decrease. The circuit depth for this experiment is 77. Fourier analysis seen in Figure 3.9 shows that already several lower frequencies have dominated the expected fifth frequency.



a



b

Fig. 3.10 Expectation values (a) and Fourier analysis (b) of experiment (3;4)

And after 4 iterations the shape of the expectation values obtained from the real device in experiment (3;4) seen in Figure 3.10 (a) barely reminds of the expected shape obtained from the simulator. The circuit depth for the experiment is 100.

It is easy to say that it was the quantum noise that messed up the picture, however, the several lower frequency dominations were not expected to such a big extent. Therefore it is left for future research to determine the cause of such behaviour. It is only assumed that layers of the quantum noise were added with each iteration in a way that introduces new frequencies and reinforces the quantum noise frequencies of the previous iterations.

### 3.1.4 Experiments on 4 qubit systems

This section describes different circuits executed and results obtained using 4 qubits with default layout from *ibmq\_5\_yorktown* backend.

Figure 3.11 shows the expectation values of experiment (4;0) and Table 3.5 describes parameters of the parametrized function (3.2) fitted with the expectation values from the real experiment. All three curves - from the simulator, the real quantum device and the fitted function - can be seen in Figure 3.11.

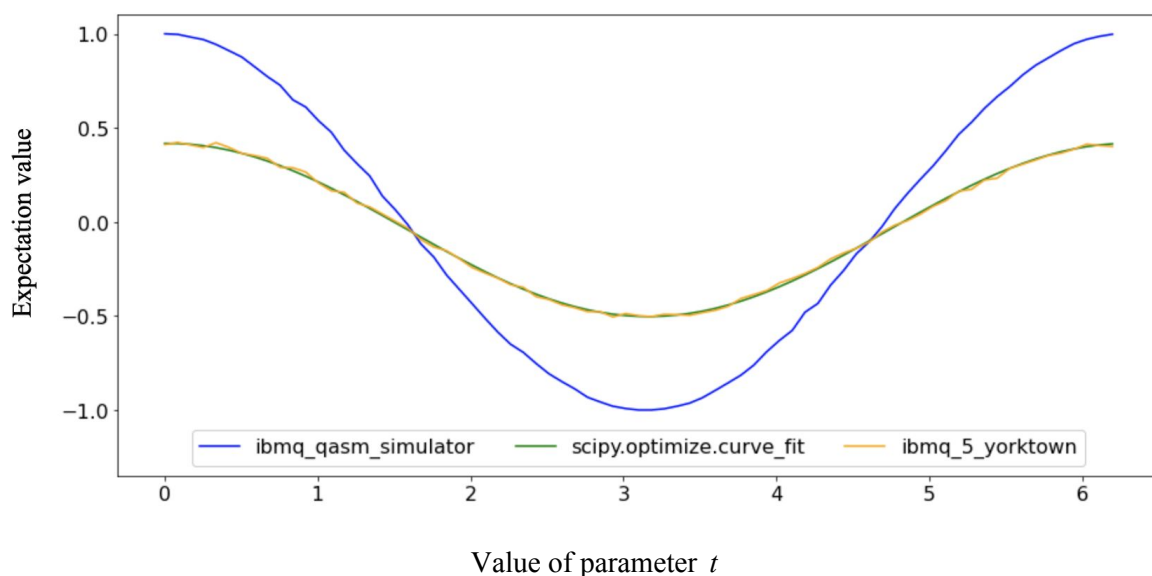


Fig. 3.11 Expectation values of experiment (4;0)

In the same way as the experiments went from the 2 qubit system described in section 3.1.2 to the 3 qubit system described in section 3.1.3, the real experiments for the 4 qubit system were performed by using one more qubit from the *ibmq\_5\_yorktown* backend. Thus, the circuit depth for experiment (4;0) is 10 and the discussion about additional errors from additional qubits described in section 3.1.3 is applicable.

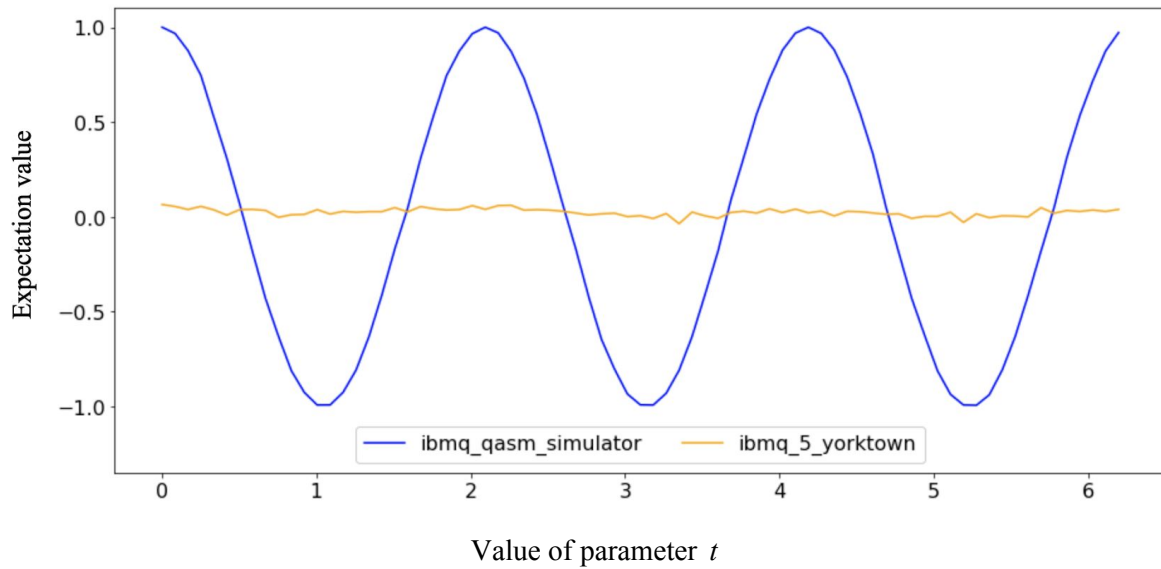
Table 3.5 Parameters of the expectation value function (3.1) fitted using results of the experiment (4;0) on *ibmq\_5\_yorktown*

$p_0$	$p_1$	$p_2$	$p_3$	MSE
0.99882	-0.01864	0.46017	-0.04229	0.00011

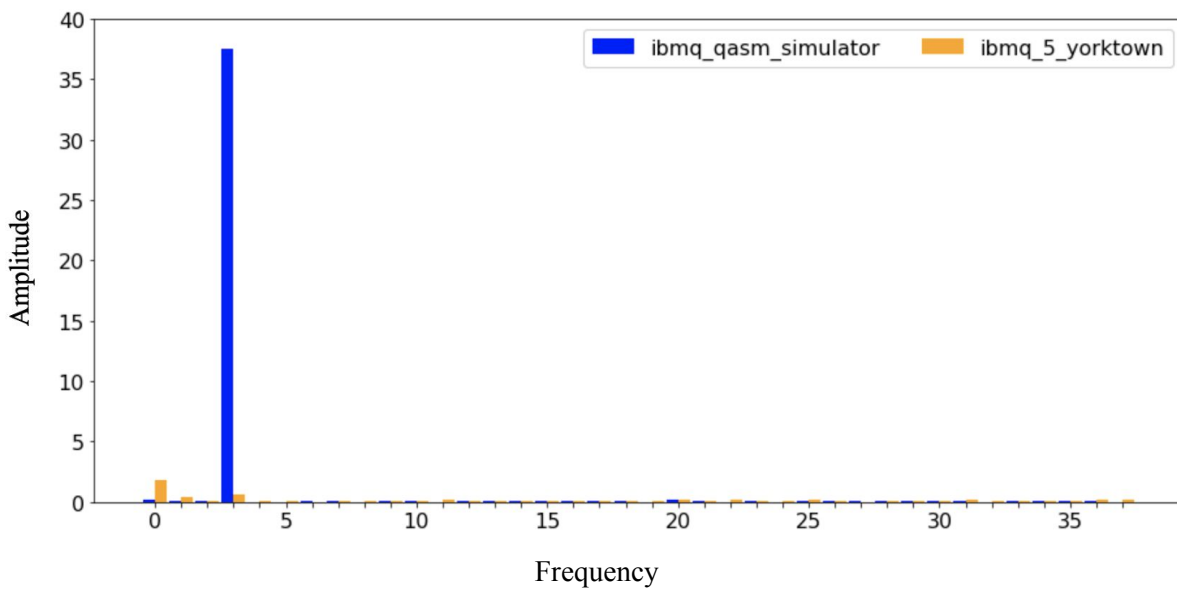
It is visible in Figure 3.11 and in the value of the parameter  $p_2$  in Table 3.5 that the amplitude dropped below a half compared to the values from the simulator with no dramatic changes in the phase difference that is quantified by the parameter  $p_3$ .

And similarly to the change in the multi-controlled NOT gate that happened between 2 qubit and 3 qubit systems, the change was made between 3 qubit and 4 qubit systems. The software developed for the research is using the *mct* gate provided by Qiskit library for all the experiments. Since Qiskit is an open-source project, it was observed from the implementation of the *mct* gate that for 2 qubits it uses a simple CNOT, for 3 qubits it uses special CCNOT gate and for a bigger number of qubits the implementation of *mct* gate depends on the mode parameter that was chosen. This thesis pushes the number of qubits to the maximum available on the *ibmq\_5\_yorktown* backend, therefore 'no ancilla' mode was selected to have a consistent *mct* gate implementation between the systems that contains more than 3 qubits.

After the first application of the Grover operator in experiment (4;1) the circuit length is 74. It can be seen in Figure 3.12 that decoherence of the system expressed by  $Z_o$  observable is critical - the curve of the expectation values obtained from the real experiment is almost flat and has nothing in common with the line observed in the simulation. Fourier analysis seen in Figure 3.12 (b) of experiment (4;1) confirms that information is almost completely lost - the dominant frequency is zero and the expected dominant frequency observed during simulation is insufficient and comparable with the first frequency that is no more than noise. **Multi-controlled Pauli-X gate seems to be the killer of the technique that eliminates all the advantages due to the complexity of the implementation.** A better implementation of  $S_0$  operator can be a savior and is a subject to a separate research.



a



b

Fig. 3.12 Expectation values (a) and Fourier analysis (b) of experiment (4;1)

Experiment (4;2) with circuit depth 156, experiment (4;3) with circuit depth 182 and experiment (4;4) with circuit depth 249 have similar pictures as the one observed in Figure 3.12, therefore they are not discussed in the section and can be found in Appendix I.

### 3.1.5 Experiments on 5 qubit systems

This section describes different circuits executed and results obtained using 5 qubits with default layout from *ibmq\_5\_yorktown* backend.

The expectation values of experiment (5;0) and the parameter values obtained by fitting the function (3.2) using expectation values obtained from the real device seen in Figure 3.13 and Table 3.6 respectively. The circuit depth is 12.

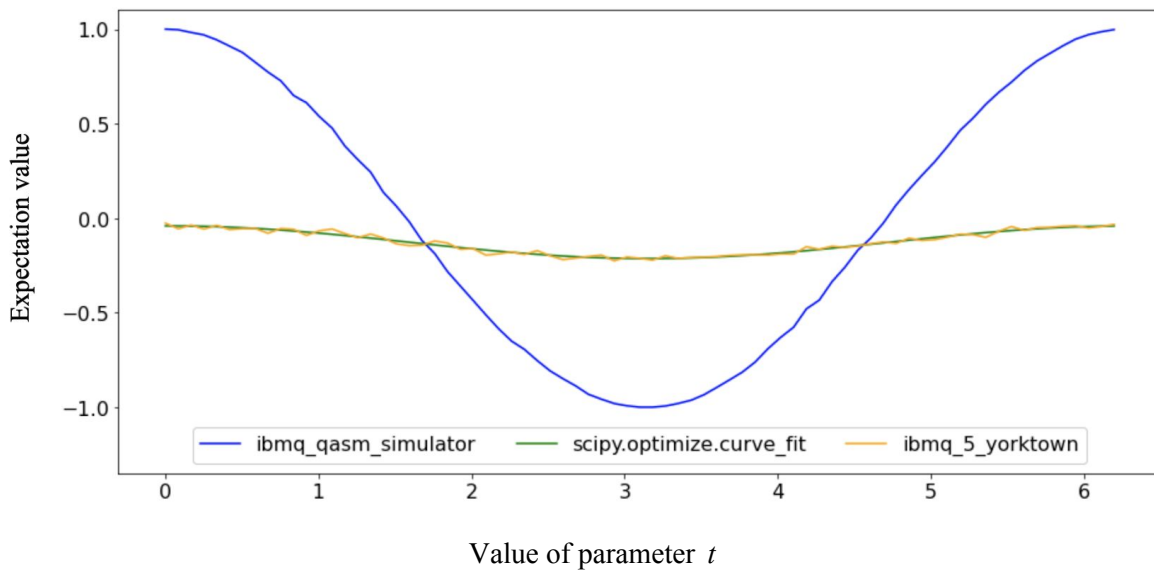


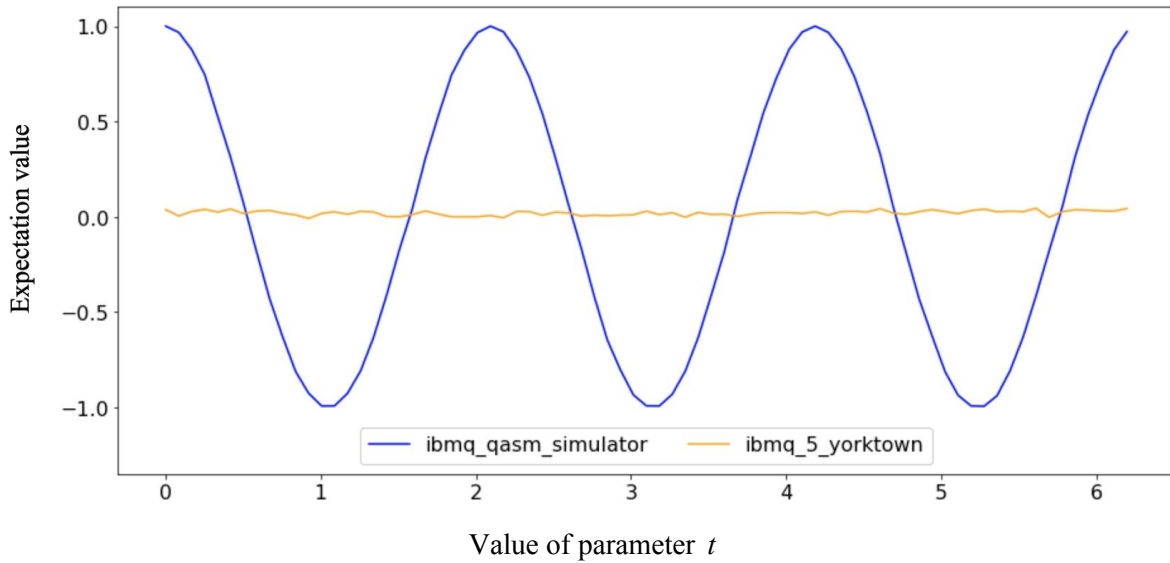
Fig. 3.13 Expectation values of experiment (5;0)

The behaviour of the results was mostly expected since the trend of adding a new qubit to the quantum system was already observed and discussed in the previous experiments on the smaller systems in sections 3.1.2 - 3.1.4.

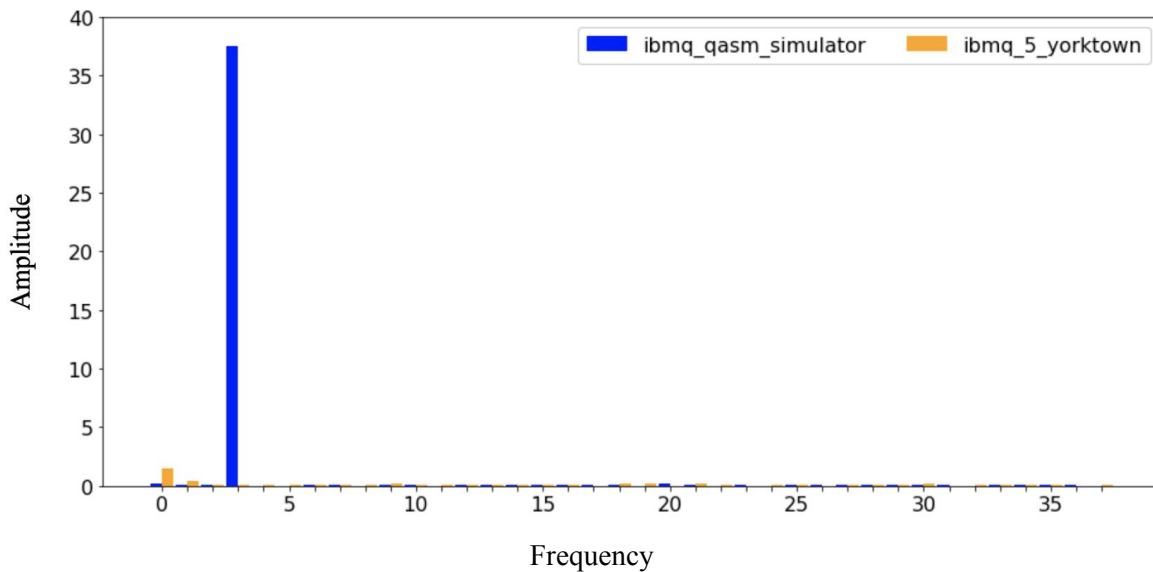
Table 3.6 Parameters of the expectation value function (3.1) fitted using results of the experiment (5;0) on *ibmq\_5\_yorktown*

$p_0$	$p_1$	$p_2$	$p_3$	MSE
1.00089	-0.02353	0.08640	-0.12671	0.00013

The gate *mtc* was used with the same parameters as for the 4 qubit system in section 3.1.4. The similar results were observed and can be seen in Figure 3.14. The circuit depth is 124.



a



b

Fig. 3.14 Expectation values (a) and Fourier analysis (b) of experiment (5;1)

After the first iteration the curve from that describes the experiment on the real quantum device is already flat indicating critical information loss - results became random. Experiments (5;2) with circuit depth 238, (5;3) with circuit depth 348 and (5;4) with circuit depth 460 are visually the same - no additional information appears in the system with the increase in the iterations. Therefore these experiments are not included in this section and can be found in Appendix I.

## 3.2 Quantum circuit fusion

This section compares and discusses application of the technique proposed by Suzuki et al. [12] to the results obtained and discussed in section 3.1.

Base on the maximization problem of Fisher information that Suzuki et al. [12] poses, it is proposed to fix number of shots  $N_{shot}$  and pick sequence of  $m_k$  values to be either linearly incremental (LIS) or exponentially incremental (EIS). When using LIS  $m_k = k$ ,  $k \geq 0$  (e.g.  $m_0 = 0, m_1 = 1, \dots$ ) and when using EIS  $m_0 = 0, m_k = 2^k, k > 0$  (e.g.  $m_0 = 0, m_1 = 2, m_2 = 4$ ). Also, it was mentioned that even though LIS can guarantee a distinct quantum advantage for estimations and EIS is asymptotically optimal for the task, the realistic performance should be analyzed. As discussed in section 3.1, systems of 4 and more qubits are losing information very quickly (almost instantly) due to quantum noise after application of the Grover operator. Thus, **the EIS regime is not realistic for NISQ devices.**

For the experiments in this section LIS regime with  $N_{shot} = 600$  was chosen to be the suitable combination that provides an exhaustive overview of the capabilities of the proposed quantum circuit fusion technique.

It was discussed in section 2.4 that IBM Quantum Experience provides a choice from a fixed set of shots number options - 1, 1024, 4096, 8192. It is obvious that one wants to have as many shots as possible to reduce statistical noise to minimum, therefore no relatively small number of shots is proposed as an option. For this thesis there was a need to reduce the number of shots in between 1 and 1024 options to see clearly the effect of the quantum fusion technique. In order to get results that represent the desired number  $N_{shot}$ , a classical software function that does “reshots” was implemented. All the results are obtained from quantum devices using 8192 shots - the maximum number of shots available at the time. It allows these experiments to keep statistical noise to the minimum that is perfect since we are interested in the effect of the quantum noise. The “reshot” function builds a set of possible system states that contains each state the same number of times as it was observed during the experiment on a real quantum device or a simulator depending on what experiment - real or simulated - needs to be “reshoted”. It allows a classical software pseudo-random number generator (PRNG) to pick a particular state with the probability close to the one observed during the real experiment. It is obvious that such a function does not represent the quantum system observation ideally, because it adds statistical noise to the one already observed during the real experiment. However, such “reshot” function can not add any quantum noise to the system, therefore this approach is good enough to simulate the desired experiment with the small  $N_{shot}$ .

Each qubit system and simulations were analysed by solving the maximization problem (2.5) for each of 75 values of the variational circuit parameter  $t$  starting from 0 applications of the

Grover operator only and then by adding one by one the circuits with 1, 2, 3 and 4 applications of the Grover operator and splitting the total number of shots  $N_{shot}$  between them. Thus the total number of shots used to obtain results remains the same. The application of the technique can be expressed as a sequence of experiments with  $m^j = \{m_0, m_1, \dots, m_j\}$ ,  $j \in [0, 1, 2, 3, 4]$ ,  $N_j = \frac{N_{shot}}{j+1}$ , where  $m^j$  is a set of circuits with a different number of iterations of the Grover operator application - from 0 to  $j$ ,  $N_j$  is the number of shots that were performed on each circuit from the set  $m^j$ . Thus, the number of shots used in total is the same  $N_{shot}$  and only the circuits in the set are different.

Function *fminbound* from SciPy library [34] was used on a negated logarithmic version of the function (2.5) in the range of  $[0; 2\pi]$  to solve the maximization problem (2.5) and obtain estimates  $\theta'_a$ . Since the trigonometric functions used in the likelihood function (2.4) can be equal to 0, the logarithm of 0 was causing a problem since it is undefined. Therefore a small number  $1e-323$  was added to the value before evaluating the logarithm. Such addition does not change the picture, thus, it does not change the solution yet allows to calculate likelihood estimations on the full range.

It was observed that the negated function (2.5) has a lot of local minimums. Numerical optimization functions from SciPy are failing to find a global minimum of this function. Therefore the minimization problem was split into minimization problems on 100 disjoint segments that represent the full range of possible values of the parameter  $t$ . From the 100 local minimums and parameter value candidates obtained the global minimum is found with the corresponding parameter value.

### 3.2.1 Application to the simulations

This section describes and illustrates how the quantum circuit fusion technique is applicable to the results obtained from simulations performed for the research to suppress statistical noise without increasing the number of shots given.

The simulations are the baseline for the research. The figures 3.15-3.18 shows how the simulation results are smoothing with the increase in the circuit set  $m^j$ .

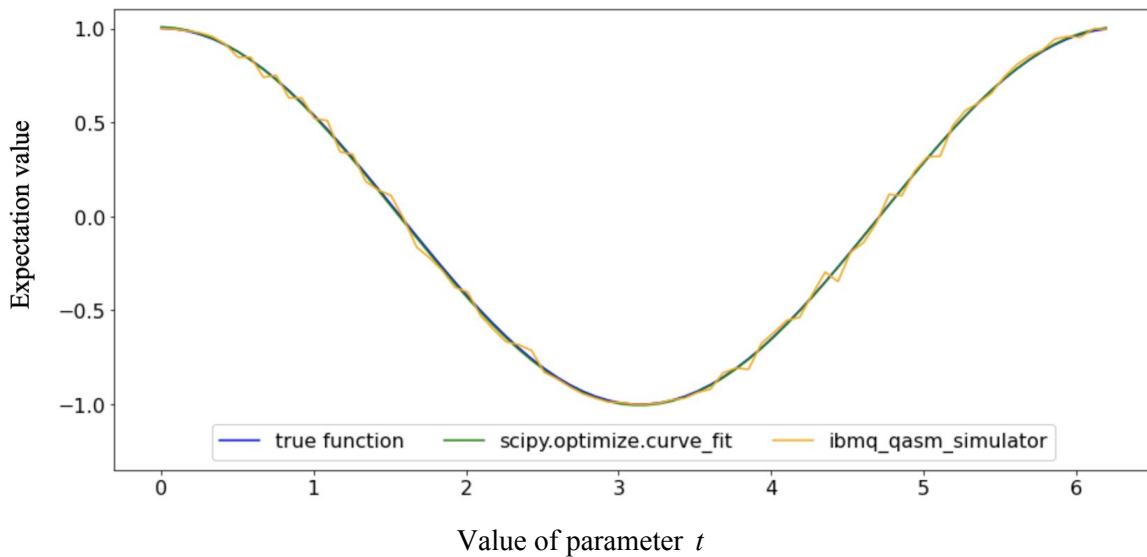


Fig. 3.15 Expectation values of the  $m^0$  circuits fusion (simulation), the function (3.2) with parameters fitted to the fusion curve (green) and the function (3.1) (blue)

Using the set  $m^0$  that contains only the original circuit the technique does not provide any improvements and does not have any advantages. It is visible in Figure 3.15 how the expectation values of the circuit jumps all the way through the curve. Nevertheless, the fitted function is close enough to the true function to obscure it.

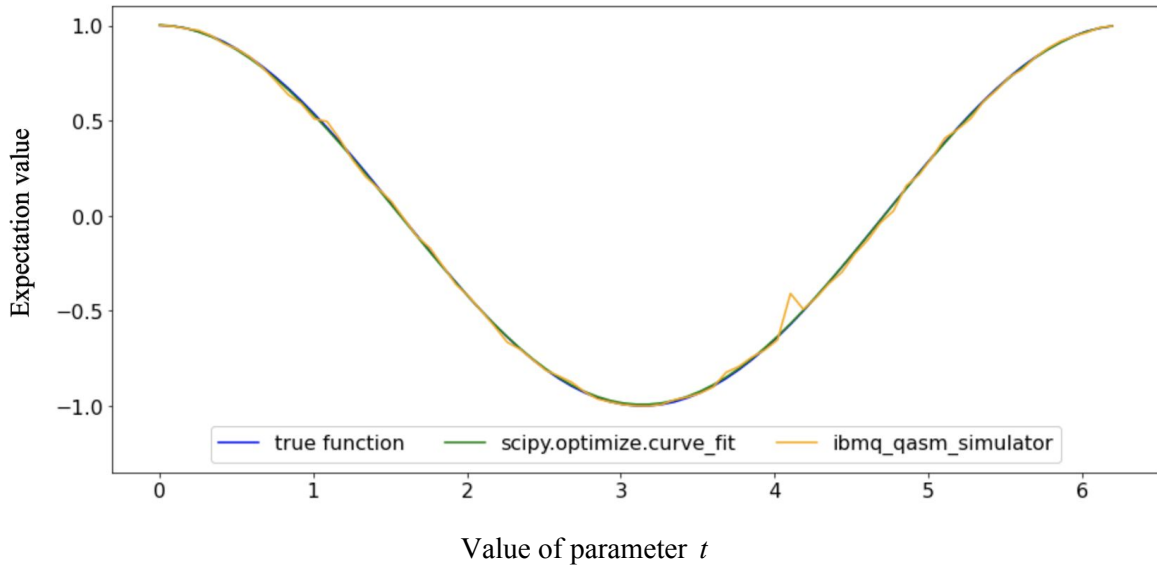


Fig. 3.16 Expectation values of simulation results with the fusion of  $m^1$  circuits (yellow), the function (3.2) with parameters fitted to the yellow curve (green) and the function (3.1) (blue)

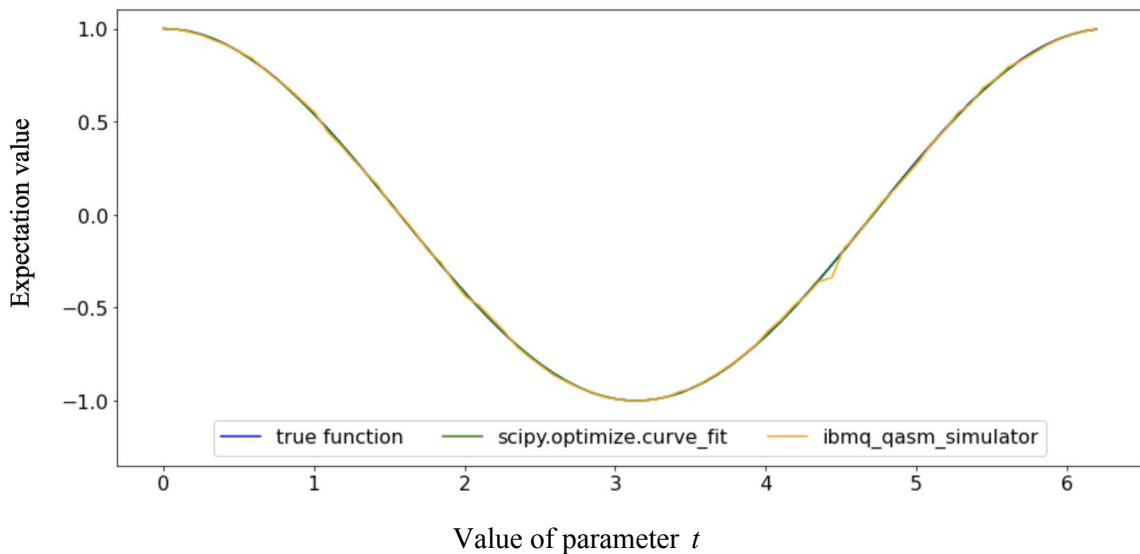


Fig. 3.17 Expectation values of simulation results with the fusion of  $m^2$  circuits (yellow), the function (3.2) with parameters fitted to the yellow curve (green) and the function (3.1) (blue)

Using the set  $m^1$  that contains additional circuit with 1 iteration of the Grover operator application over the set  $m^0$  the expectation values of the experiments became more smooth as seen in Figure 3.16, though a sufficient deviation from the true function is visible in the region of  $t = 4.1$ . Using the set  $m^2$  that also contains one more circuit with 2 iterations of the Grover operator application over the set  $m^1$  the expectation values continue smoothing towards the true function as seen in the Figure 3.17.

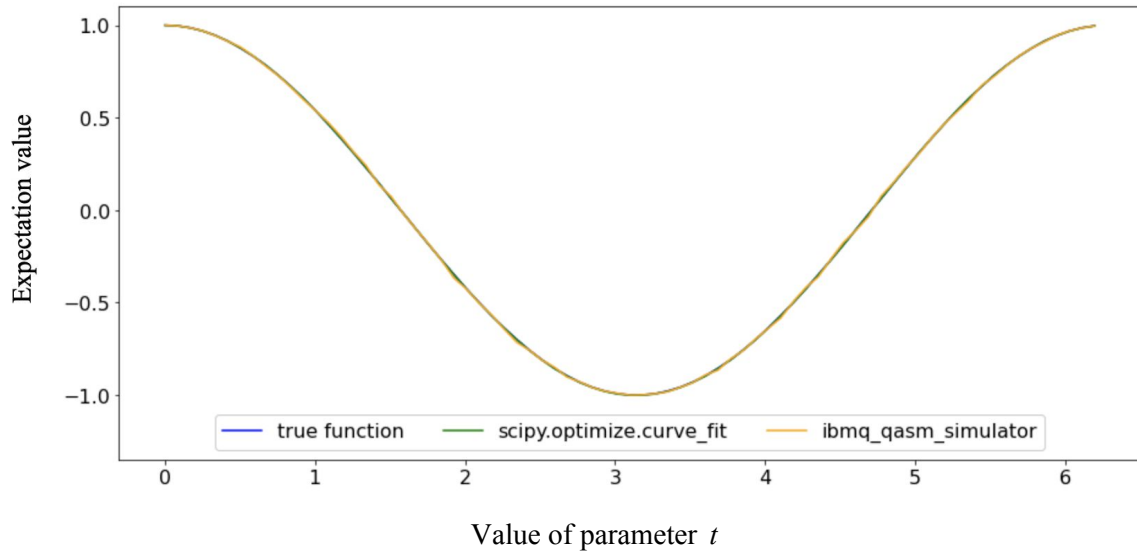


Fig. 3.18 Expectation values of simulation results with the fusion of  $m^3$  circuits (yellow), the function(3.2) with parameters fitted to the yellow curve (green) and the function (3.1) (blue)

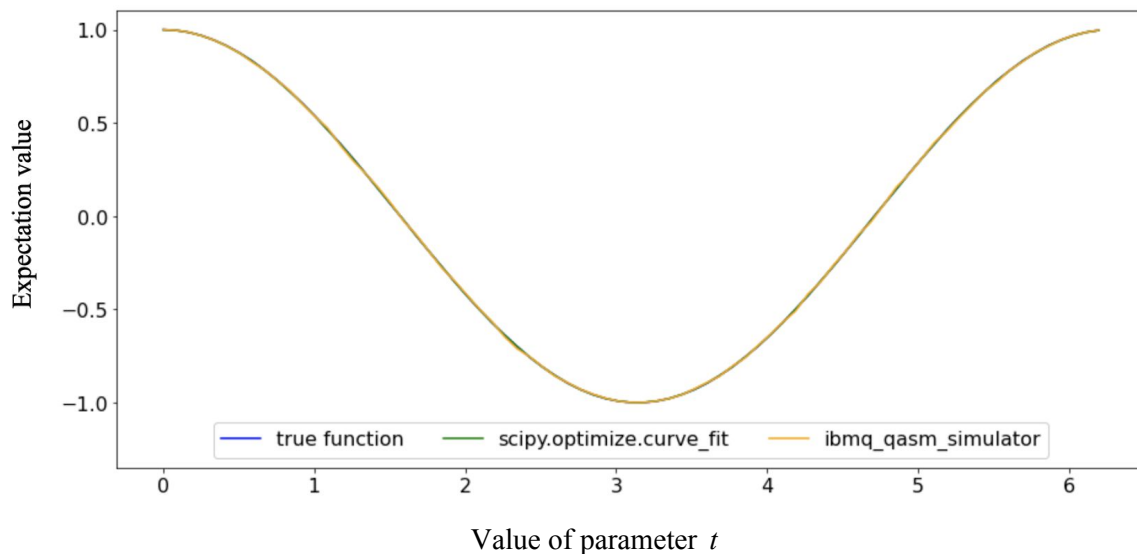


Fig. 3.19 Expectation values of simulation results with the fusion of  $m^4$  circuits (yellow), the function (3.2) with parameters fitted to the yellow curve (green) and the function (3.1) (blue)

Using the set  $m^3$  the expectation values from the experiments almost fully obscure the true function. It is important to remember that the total number of shots is the same for all the sets, the shots are just used differently - e.g. when using the set  $m^0$  all the  $N_{shot}$  shots are used to run the original circuit without any Grover operator applications, when using the set  $m^3$  that contains 4 different circuits only  $\frac{N_{shot}}{4}$  shots are used to run the original circuit and other shots are also divided equally to obtain results from the rest of the circuits in the set.

Table 3.7 Parameters of the expectation value function (3.2) fitted to the fusion of  $m^j$  circuits (simulation)

$j$	$p_0$	$p_1$	$p_2$	$p_3$	MSE
0	0.99549	0.01786	1.00690	0.00136	0.00072
1	0.99400	0.02095	0.99731	0.00555	0.00050
2	0.99835	0.00330	1.00008	0.00009	0.00013
3	1.00078	-0.00269	1.00032	-0.00142	0.00004
4	0.99971	0.00102	0.99939	0.00011	0.00002

And finally, the expectation values from the set  $m^4$  - the smoothest curve from all the figures - can be seen in Figure 3.19. The fitted parameter values of the parametrized expectation function (3.2) for each circuit set can be seen in Table 3.7. The values in the table confirm that parameters converge to the parameters of the true function with the increase of circuits with different number of iterations of the Grover operator application in the set that is used to perform the quantum circuit fusion without any increase in the number of shots given for a set. In fact, the parameters in Table 4.4 for  $j = 4$  obtained using only 600 shots and the quantum circuit fusion technique are closer to the true function (3.1) than the simulation results in Table 3.2 obtained using 8192 shots to run only the original circuit. It means **better results with over 13 times reduction in the number of circuit executions.**

### 3.2.1 Application to the 2 qubit circuit

This section describes and illustrates how the quantum circuit fusion technique behaves on the 2 qubit system experiments.

It was shown in section 3.2.2 that the quantum circuit fusion technique on a simulator achieves outstanding results in statistical noise suppression. Now the question is if the technique is capable of performing efficiently in the presence of quantum noise.

Figures 3.20-3.24 show the behaviour of the quantum circuit fusion technique on different sets of the circuits with different number of iterations of the Grover operator application with the fixed number  $N_{shot} = 600$  available to perform on each set of circuits  $m^j$ .

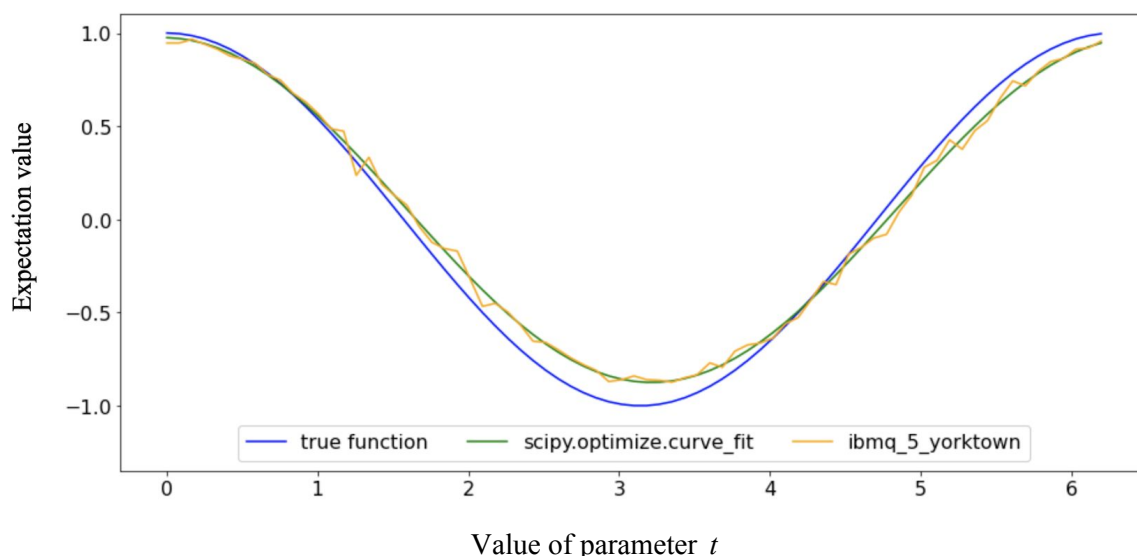


Fig. 3.20 Expectation values of the  $m^0$  circuits fusion (2 qubit system), the function (3.2) with parameters fitted to the fusion curve (green) and the function (3.1) (blue)

Using the set  $m^0$  defined in the beginning of section 3.2 gains expectation values similar to the results of experiment (2;0) that can be seen in Figure 3.1 - the curve is shifted to the right from the true function and amplitude is lower than the one of the true function. It indicates that the quantum noise of experiment (2;0) is still present. However, the statistical noise is worse due to the reduced number of shots compared to experiment (2;0). It is visible in the roughness of the curve that jumps up and down in the region of the fitted function that does not have the axis of freedom to jump similarly to the real curve and, thus, behaves smoothly as seen in Figure 3.20. As expected, no advantages are observed.

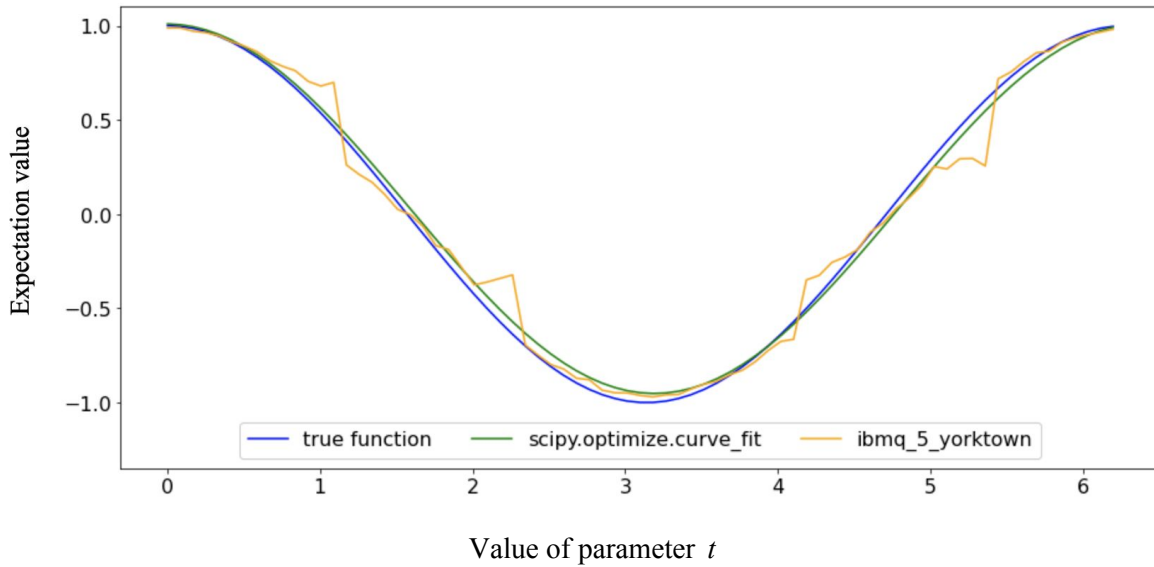


Fig. 3.21 Expectation values of the  $m^1$  circuits fusion (2 qubit system), the function (3.2) with parameters fitted to the fusion curve (green) and the function (3.1) (blue)

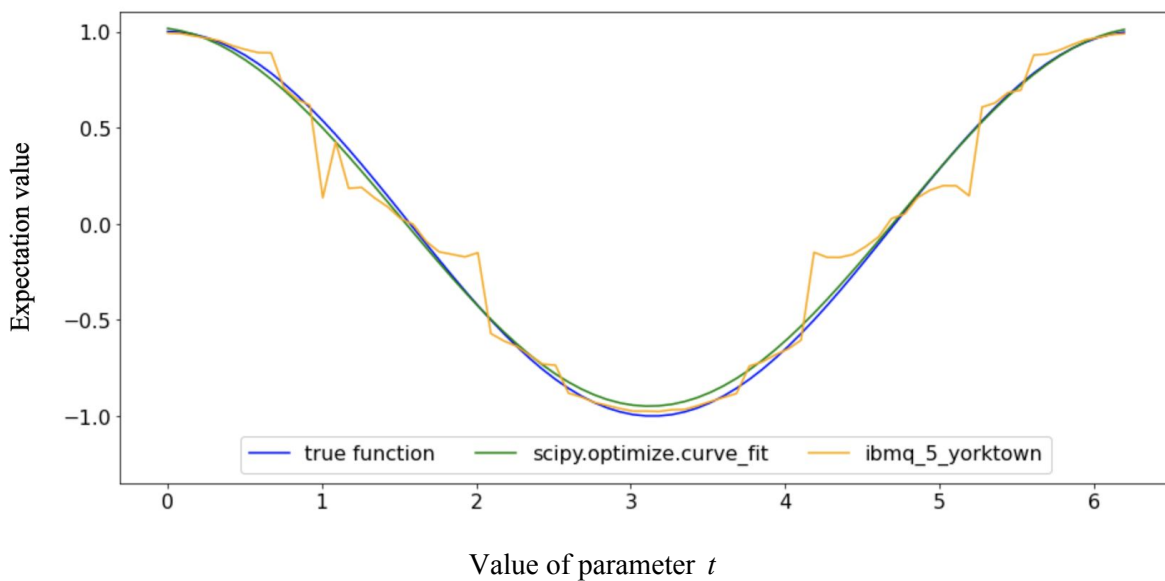


Fig. 3.22 Expectation values of the  $m^2$  circuits fusion (2 qubit system), the function (3.2) with parameters fitted to the fusion curve (green) and the function (3.1) (blue)

When using sets  $m^1$  and  $m^2$  to perform the quantum circuit fusion, expectation values from the experiment become more smooth in between the points. Nevertheless, the curve deviates sufficiently from the fitted curve and the true function compared to the expectation values seen in Figure 3.20.

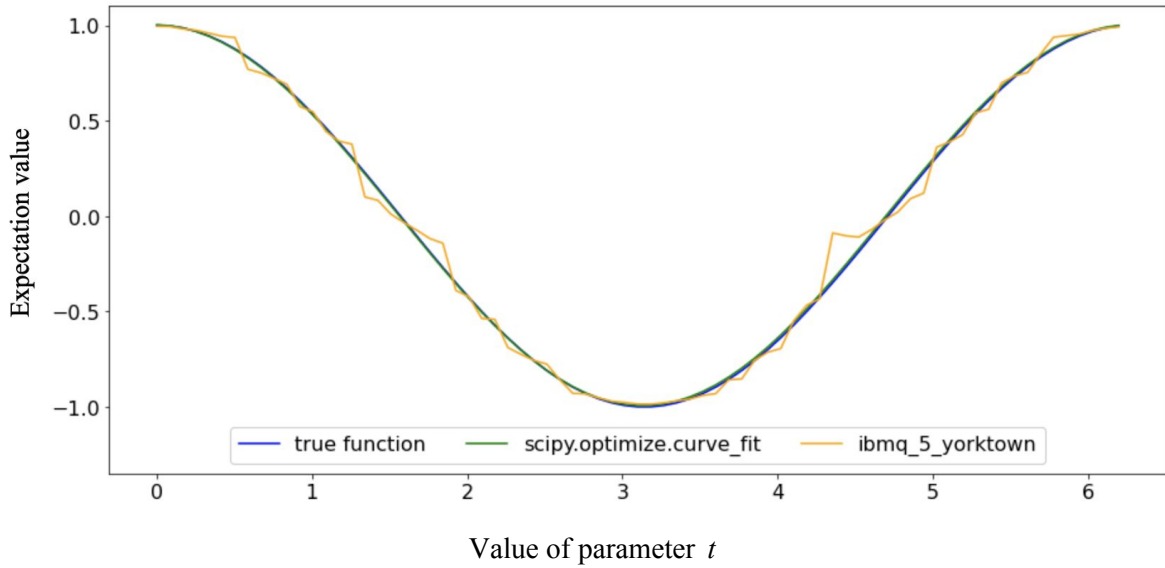


Fig. 3.23 Expectation values of the  $m^3$  circuits fusion (2 qubit system), the function (3.2) with parameters fitted to the fusion curve (green) and the function (3.1) (blue)

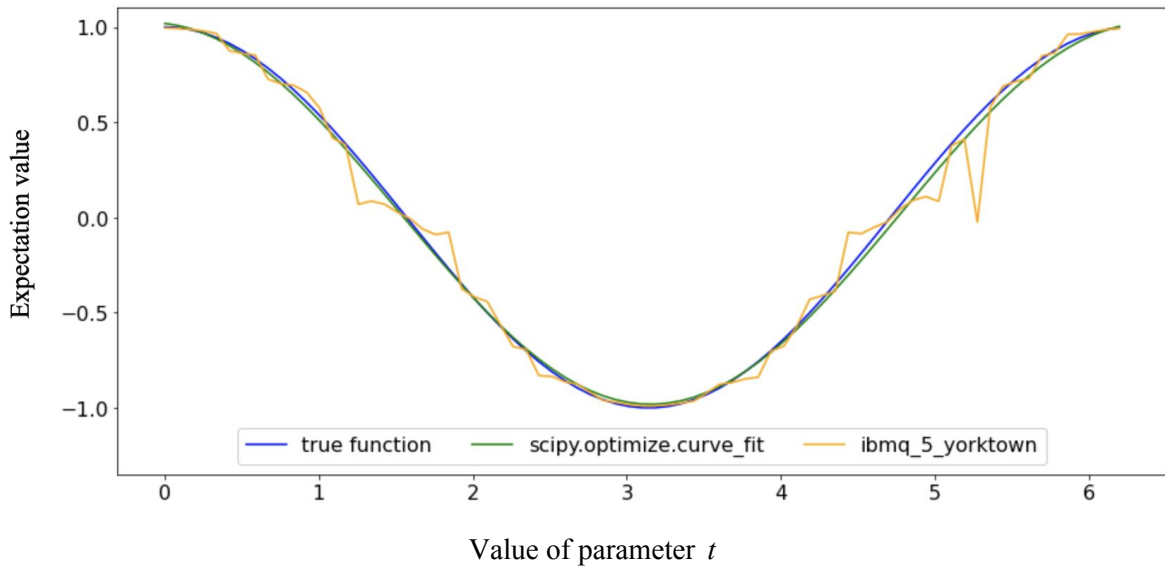


Fig. 3.24 Expectation values of the  $m^4$  circuits fusion (2 qubit system), the function (3.2) with parameters fitted to the fusion curve (green) and the function (3.1) (blue)

The same outstanding deviations can be seen in the figures 3.16-3.17 of the simulations in the region of  $t = 4.5$ . It may be some drawback of the implementation chosen that was amplified by the quantum noise present in the real experiment or it may be some drawback of the technique itself when using a small number of circuits during fusion. The question is not in the scope of this research and can be studied separately.

What is interesting, when using  $m^3$  set to obtain expectation values it can be seen in Figure 3.23 that the fitted curve is the closest to the true function - the amplitude and phase differences were suppressed. Though the noise is still sufficient the curve is visibly better than in Figure 3.21 and Figure 3.22. However, when expanding the set to  $m^4$  noise deviations are increased again. The experiment was repeated several times and all of the times the noise in the results of  $m^4$  set fusion are visually worse than the results of  $m^3$  set fusion.

The fitted parameters of the parametrized expectation value function (3.2) confirms the finding of the visual analysis performed and can be seen in Table 3.8. From  $j = 0$  to  $j = 3$  amplitude and shift are getting better towards the true function and when  $j = 4$  the curve is getting worse - away from the true function.

Table 3.8 Parameters of the expectation value function (3.2) fitted to the fusion of  $m^j$  circuits (2 qubit system)

$j$	$p_0$	$p_1$	$p_2$	$p_3$	MSE
0	0.96998	0.02124	0.92511	0.05035	0.00104
1	0.98123	0.00969	0.98050	0.02888	0.00668
2	0.97222	0.10635	0.98509	0.03658	0.00982
3	0.99950	0.01199	0.99766	0.00468	0.00275
4	0.96681	0.09122	1.00173	0.02113	0.00756

To summarize, the quantum circuit fusion technique has not performed as well as in the simulation. Nevertheless, it was able to improve the common problems observed during the experiment on a real quantum device - pulses imprecision and system decoherence that were assumed to be the cause of the differences in amplitudes and phases compared to the simulations.

### 3.2.2 Application to the 3 qubit circuit

This section describes and illustrates how the quantum circuit fusion technique behaves on the 3 qubit system experiments.

It was shown in section 3.2.1 that the quantum fusion technique was capable of providing some improvements over the original experiments even in the presence of a lower number of shots available. Nevertheless, results have not shown any stable noise diminishing with the changes in the circuit set used to perform quantum circuit fusion.

When applying the technique with different circuit sets to the 3 qubit system, completely different results were observed. These results are illustrated in the figures 3.25-3.27.

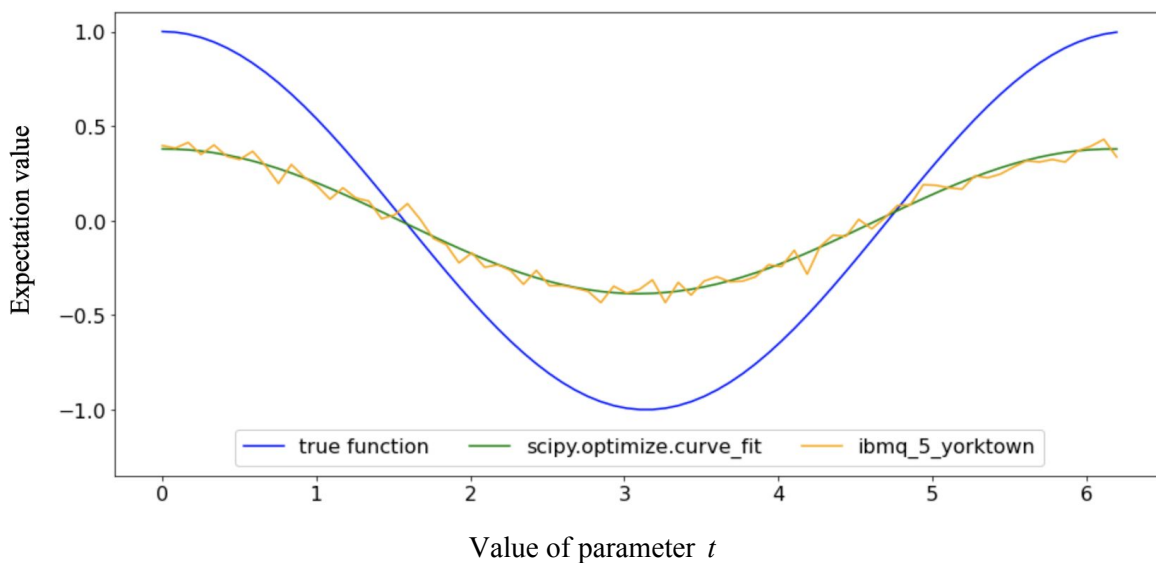


Fig. 3.25 Expectation values of the  $m^0$  circuits fusion (3 qubit system), the function (3.2) with parameters fitted to the fusion curve (green) and the function (3.1) (blue)

The usage of the  $m^0$  circuit set shows once more that the essence of the original experiment (3;0) is present in the shape of the curve - the amplitude is lower than the amplitude of the true function more than in a half - and the statistical noise increased with the decrease in the number of shots. The expectation values in Figure 3.25 are not as smooth as the expectation values of experiment (3;0) seen in Figure 3.6.

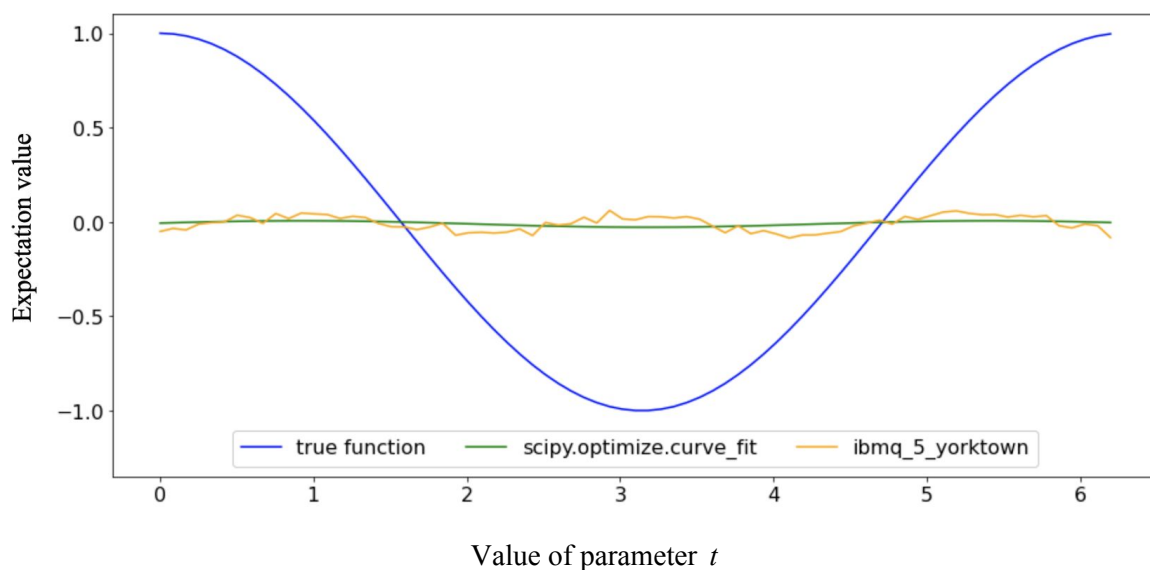


Fig. 3.26 Expectation values of the  $m^1$  circuits fusion (3 qubit system), the function (3.2) with parameters fitted to the fusion curve (green) and the function (3.1) (blue)

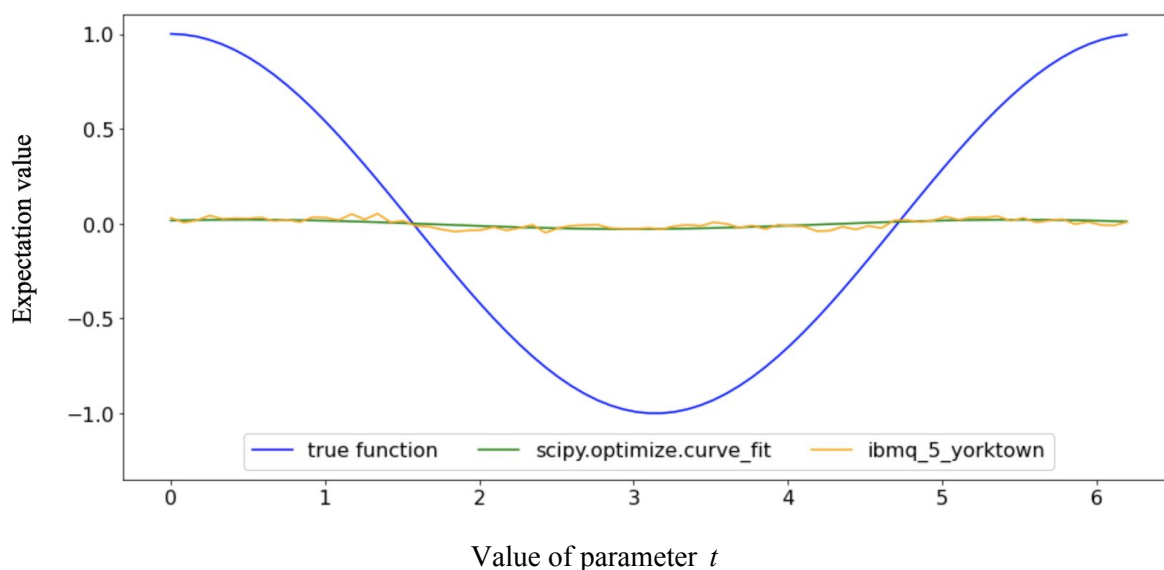


Fig. 3.27 Expectation values of the  $m^2$  circuits fusion (3 qubit system), the function (3.2) with parameters fitted to the fusion curve (green) and the function (3.1) (blue)

Surprisingly, the usage of the  $m^1$  and  $m^2$  sets completely erases all the information - the curve seen in Figure 3.26 and Figure 2.27 is completely flat. The similar results were obtained during the fusion of  $m^3$  and  $m^4$  sets, therefore they are not included in the section and can be found in Appendix I.

Experiments on 3 qubit systems contained a lot of lower frequencies with significant amplitudes supposedly caused by the quantum noise that was introduced with the increased complexity of the *mtc* gate discussed in section 3.1.3. These noise frequencies seem to affect the fusion technique dramatically.

Table 3.9 Parameters of the expectation value function (3.2) fitted to the fusion of  $m^j$  circuits (3 qubit system)

$j$	$p_0$	$p_1$	$p_2$	$p_3$	MSE
0	1.02084	-0.01413	0.38264	-0.00354	0.00146
1	1.39907	-1.29592	0.01707	-0.01077	0.00137
2	1.25602	-0.60243	0.02441	-0.00401	0.00029
3	2.97528	-3.13230	0.00726	-0.00075	0.00013
4	1.02344	-3.77350	-0.00073	0.00219	0.00008

The fitted parameters of the parametrized expectation value function (3.2) for each circuit set can be seen in Table 3.9. The significant drop in the amplitude quantified by the parameter  $p_2$  can be observed with the increase in the value of the parameter  $j$ . Other parameters are not meaningful in the presence of the low amplitude.

To summarize, the quantum fusion technique was absolutely not applicable for the experiments on the 3 qubit system.

### 3.2.3 Application to the 4 and 5 qubit circuits

This section describes and illustrates how the quantum circuit fusion technique behaves on the 4 and 5 qubit systems experiments.

The technique application totally failed with the grown complexity of the system which entailed the growth in complexity of *mct* gate required for the implementation of the operator  $S_0$  chosen for this research. The system gets more complex once more with the introduction of the fourth qubit and consecutive change in the *mct* calculation algorithm that was observed in the source code of Qiskit.

Surprisingly, the results of the technique application to the 4 qubits systems were nothing like the results obtained for the smaller systems. The results can be seen in the figures 3.30-3.34.

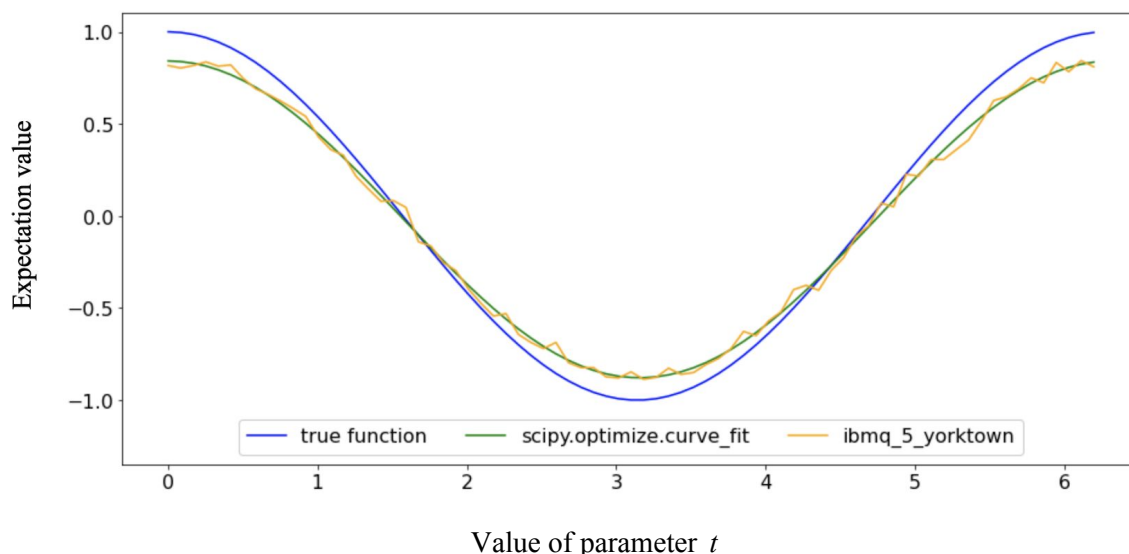


Fig. 3.30 Expectation values of the  $m^0$  circuits fusion (4 qubit system), the function (3.2) with parameters fitted to the fusion curve (green) and the function (3.1) (blue)

The quantum circuit fusion technique used on the set  $m^0$  gains the similar results to the original experiment (4;0) with more pronounced statistical noise. The noticeable difference is the amplitude that was improved toward the true function in comparison with the original experiment (4;0) depicted in Figure 3.11.

For the circuit sets where the Grover operator was used, there was a need to increase the maximum number of iterations (*maxfev* parameter) for the *fminbound* function. The function was not capable of reaching optimal values with the default maximum number of iterations.

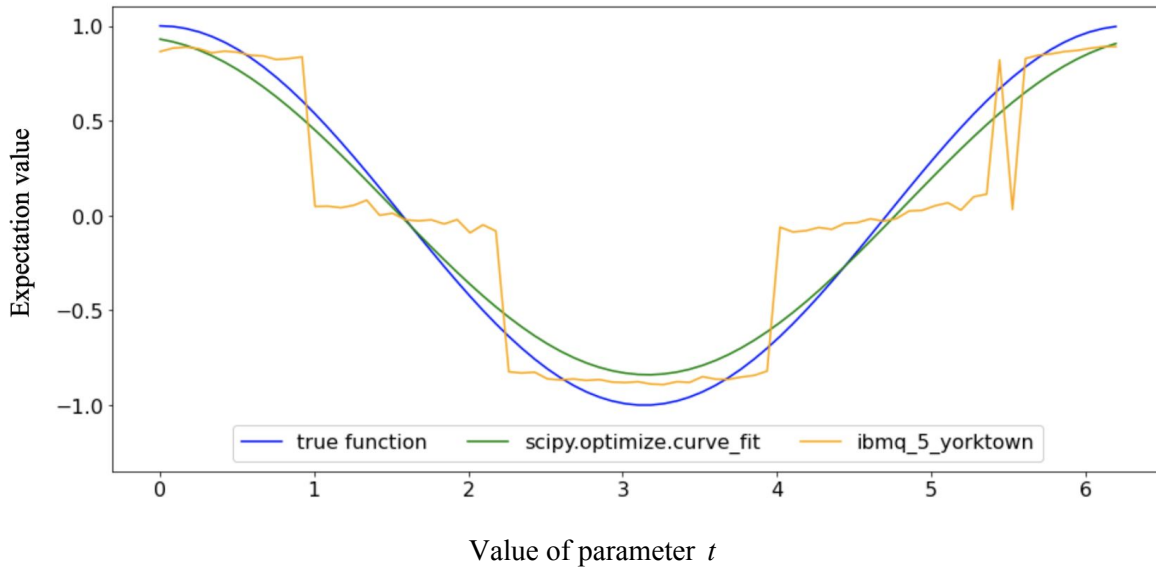


Fig. 3.31 Expectation values of the  $m^1$  circuits fusion (4 qubit system), the function (3.2) with parameters fitted to the fusion curve (green) and the function (3.1) (blue)

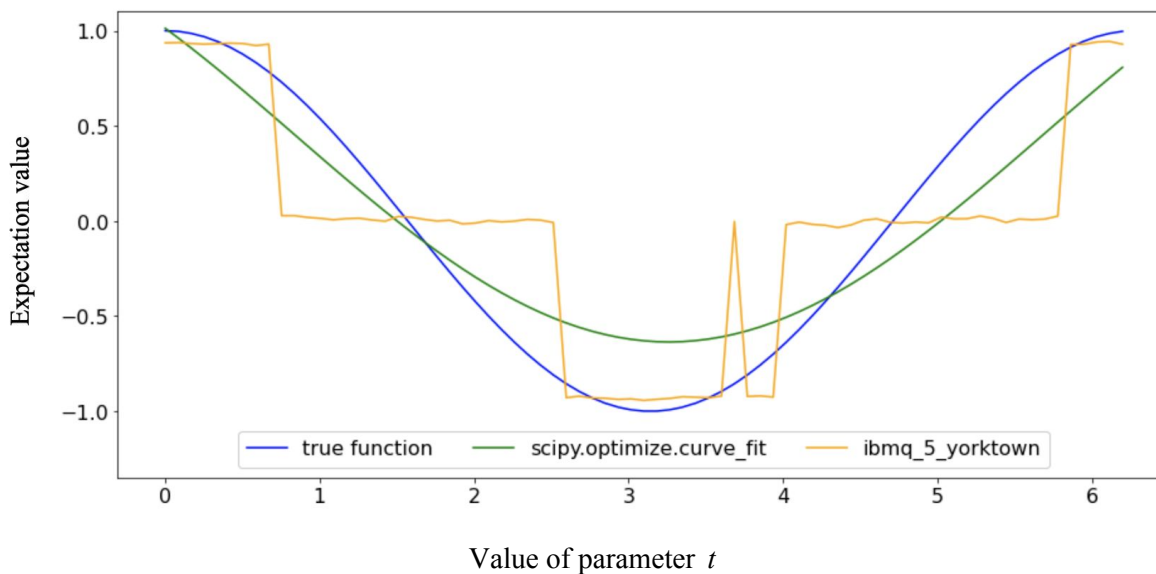


Fig. 3.32 Expectation values of the  $m^2$  circuits fusion (4 qubit system), the function (3.2) with parameters fitted to the fusion curve (green) and the function (3.1) (blue)

When using the technique with  $m^1$  and  $m^2$  circuit sets it can be seen in Figure 3.31 and Figure 3.32 that a separate regions of the values of the parameter  $t$  collapses to constant expectation values - either close to 1, 0 and -1. The expectation value function at this point resembles a step function. It may be due to the fact the circuit depth is so high that the expectation values of the original experiments (4;1) and (4;2) already become flat. These

circuits with the flat results reassure the technique that in the regions where expectation value is close to 0 the true expectation value must be 0 - thus the plateaus are formed with the expectation value 0. Nevertheless, the technique is still capable of picking up the information at the regions with the maximum amplitude of the expectation values and the algorithm smooths out the rest of the curvature - thus the plateaus are formed with the expectation values 1 and -1.

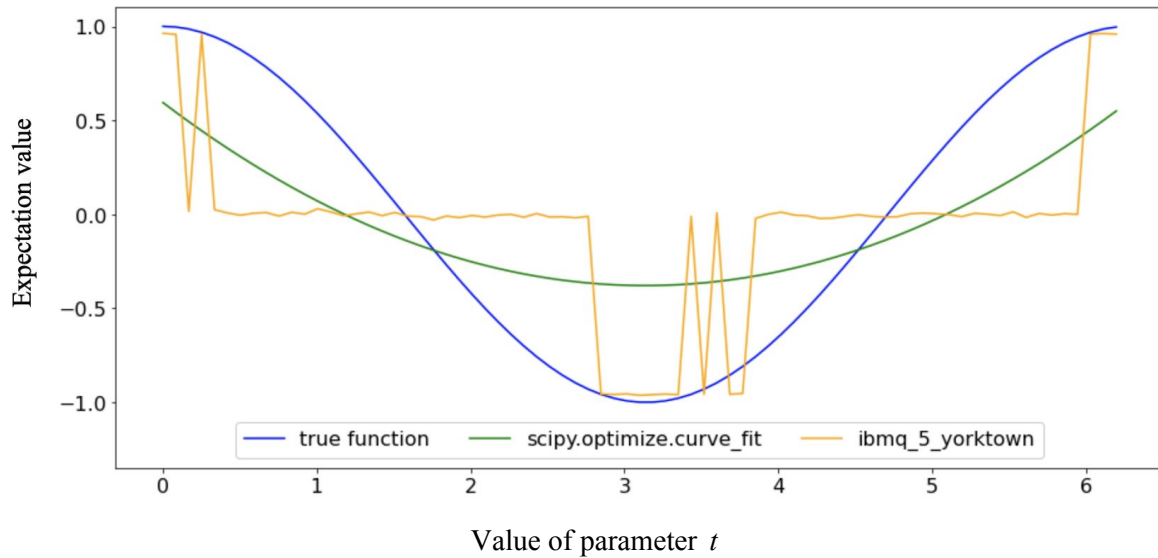


Fig. 3.33 Expectation values of the  $m^3$  circuits fusion (4 qubit system), the function (3.2) with parameters fitted to the fusion curve (green) and the function (3.1) (blue)

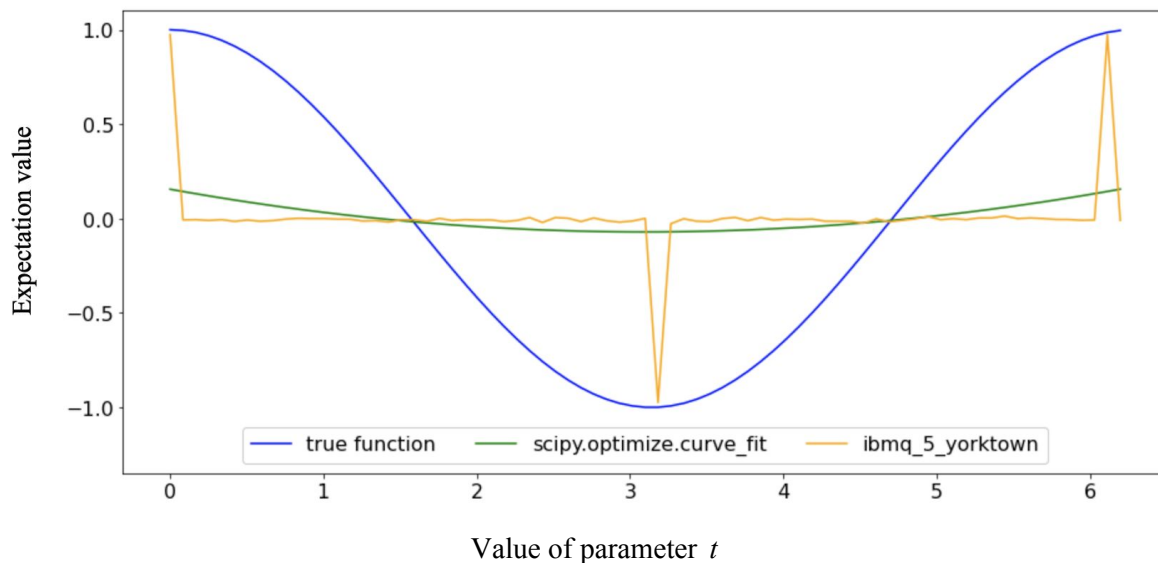


Fig. 3.34 Expectation values of the  $m^4$  circuits fusion (4 qubit system), the function (3.2) with parameters fitted to the fusion curve (green) and the function (3.1) (blue)

The similar picture, but with progressing information loss, can be seen in Figure 3.33 and Figure 3.34 where sets  $m^3$  and  $m^4$  were used. The fitted parameters of the parametrized expectation value function (3.2) for each circuit set can be seen in Table 3.10. The parameters quantify the increase in the amplitude that was obtained on the set  $m^0$  and all the other parameters for  $j > 0$  shows the decay that was visually observed in the figures 3.31-3.34 and MSE values show how the function (3.2) is poorly capable of representing the outrageous expectation value function from the experiments.

Table 3.10 Parameters of the expectation value function (3.2) fitted to the fusion of  $m^j$  circuits (4 qubit system)

$j$	$p_0$	$p_1$	$p_2$	$p_3$	MSE
0	0.99366	0.00372	0.86015	-0.01848	0.00105
1	0.94331	0.15699	0.89019	0.05056	0.04474
2	0.65141	1.01678	1.08013	0.44450	0.09393
3	0.01740	3.08703	653.91099	653.53230	0.10827
4	0.00892	3.11394	591.30655	591.23590	0.03318

Application of the quantum fusion technique for the 5 qubit system has exactly the same results and does not add anything new to the picture that was not already observed in the experiment for the 4 qubit system. Therefore the experiments for the 5 qubit system were not included in the section and can be found in Appendix I.

To summarize, the circuit fusion technique fails for deep circuits. It was expected considering the expectation values that were obtained from these circuits in section 3.1. These values show that all the information in the system was lost and thus, the circuits only harm results during the fusion procedure.

## 4 Conclusion

The research was aimed to investigate the efficiency of the quantum fusion technique on the NISQ devices. In this thesis, the technique was applied to the circuits executed on `ibmq_qasm_simulator` and `ibmq_5_yorktown` devices publicly available via IBM Quantum Experience cloud platform. A diverse set of experiments was prepared and performed using variational quantum circuits that were built for 2, 3, 4 and 5 qubit systems with 0 to 4 iterations of Grover operator application. The outcomes of the technique application were analysed and discussed.

The research showed and quantified the noise that is present when performing quantum computations. Fourier analysis in a form of parameters fitting and in a form of frequency analysis revealed and quantified the difference in noise between simulations and experiments on a real quantum device. It was observed how with the increase of circuit depth and with the increase in system complexity the output of the real quantum computer introduces new frequencies into results and loses amplitude of the expected frequencies. These results demonstrate the essence of the quantum computation problems and the actuality of the research in the field of quantum noise suppression.

The simulations were used as a baseline due to the absence of quantum noise and the presence of the statistical noise only. It was visible that any signs of quantum noise, such as rotation imprecision and decoherence, are completely absent in the simulations. It was also shown how the statistical noise amplifies with the reduction in the number of shots. The quantum fusion technique using the same amount of shots achieved significant statistical noise suppression by distributing shots among a set of circuits with different numbers of Grover iterations. It was shown that in the absence of quantum noise, the technique is capable of outperforming the baseline experiment that used more than 13 times more shots with only 5 different circuits in the fusion set.

Nevertheless, **the quantum circuit fusion technique gave doubtful results on a very small 2 qubit system and completely failed on the still small yet bigger quantum systems of 3, 4 and 5 qubits.**

The quantum noise was observed in every circuit. Fourier analysis allowed the research to quantify the phase shift and the amplitude reduction during experiments on the real quantum computer. It was proposed that the cause of the phase shift may be in the pulses imprecision that are used to rotate qubits and the cause of the amplitude reduction may be in the decoherence of the quantum system which starts to lose encoded information with time.

Severe information loss was observed when running deep quantum circuits that contain a lot of entanglement between qubits. The expectation values of the results of the variational circuit of depth over 70 were close to 0 regardless of the parameter value for 4 and 5 qubit systems that indicates complete information loss.

When using the technique on the 2 qubits system, a quantum noise correction effect was observed in phase and amplitude. It is uncertain if the observed phenomena was a property of the technique - a separate study needs to be performed. Nevertheless, no sufficient improvements other than the expectation values curve smoothing were observed. When using the technique on the 3, 4 and 5 qubit systems, additional circuits that show full information loss or other severe quantum noise manifestations when added to the fusion set only harms the outcome.

It was determined in the research that the technique is viable for NISQ devices if and only if an efficient implementation of Grover operator is found. As a future research, a better implementation of Grover operator can be analysed.

## References

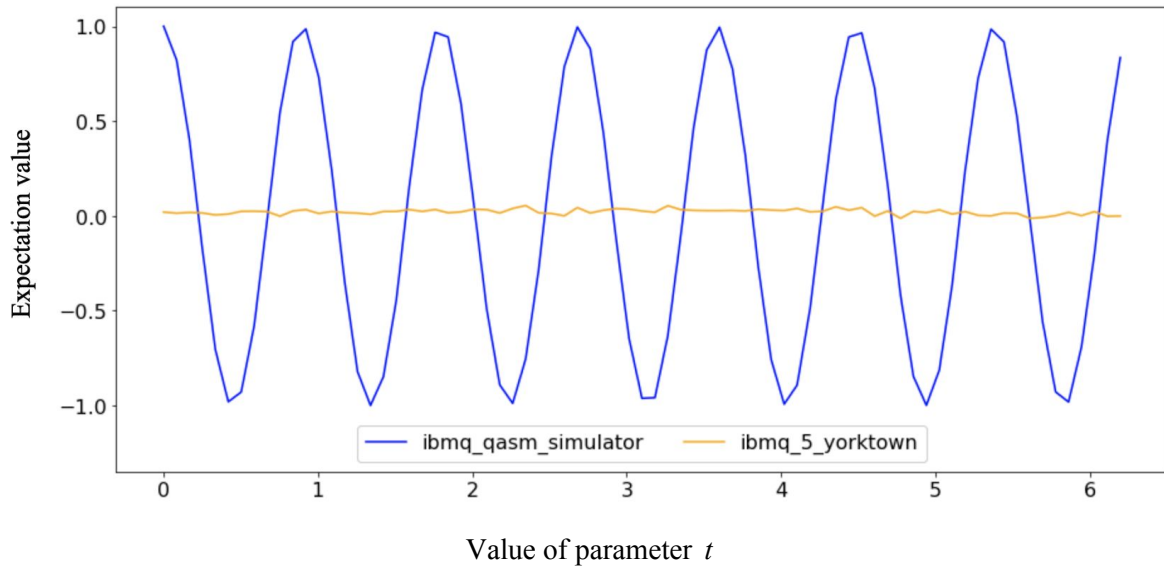
- [1] Preskill, J. (2018). Quantum Computing in the NISQ era and beyond. *Quantum*, 2, 79.
- [2] Knill, E., Ortiz, G., & Somma, R. D. (2007). Optimal quantum measurements of expectation values of observables. *Physical Review A*, 75(1), 012328.
- [3] Brassard, G., Hoyer, P., Mosca, M., & Tapp, A. (2002). Quantum amplitude amplification and estimation. *Contemporary Mathematics*, 305, 53-74.
- [4] IBM Quantum Experience platform.  
<https://quantum-computing.ibm.com>
- [5] Kitaev, A. Y., Shen, A., Vyalyi, M. N., & Vyalyi, M. N. (2002). Classical and quantum computation (No. 47). American Mathematical Soc..
- [6] Svore, K. M., Hastings, M. B., & Freedman, M. (2013). Faster phase estimation. arXiv preprint arXiv:1304.0741.
- [7] Wiebe, N., & Granade, C. (2016). Efficient Bayesian phase estimation. *Physical review letters*, 117(1), 010503.
- [8] Poulin, D., Kitaev, A., Steiger, D. S., Hastings, M. B., & Troyer, M. (2018). Quantum algorithm for spectral measurement with a lower gate count. *Physical review letters*, 121(1), 010501.
- [9] Parrish, R. M., & McMahon, P. L. (2019). Quantum Filter Diagonalization: Quantum Eigendecomposition without Full Quantum Phase Estimation. arXiv preprint arXiv:1909.08925.
- [10] Somma, R. D. (2019). Quantum eigenvalue estimation via time series analysis. *New Journal of Physics*, 21(12), 123025.
- [11] Svore, K. M., Hastings, M. B., & Freedman, M. H. (2016). U.S. Patent No. 9,275,011. Washington, DC: U.S. Patent and Trademark Office.
- [12] Suzuki, Y., Uno, S., Raymond, R., Tanaka, T., Onodera, T., & Yamamoto, N. (2020). Amplitude estimation without phase estimation. *Quantum Information Processing*, 19(2), 75.
- [13] Qiskit quantum computing software development framework, version 17.1.  
<https://qiskit.org>
- [14] 5-qubit backend: IBM Q team, "IBM Q 5 Yorktown backend specification V2.0.5", (2020).  
Retrieved from <https://quantum-computing.ibm.com>

- [15] Up to 32 qubits simulation backend: IBM Q team, "IBM Q QASM simulator backend specification V0.1.547", (2020).  
Retrieved from <https://quantum-computing.ibm.com>
- [16] Brassard, G., & Hoyer, P. (1997, June). An exact quantum polynomial-time algorithm for Simon's problem. In Proceedings of the Fifth Israeli Symposium on Theory of Computing and Systems (pp. 12-23). IEEE.
- [17] Grover, L. K. (1998). Quantum computers can search rapidly by using almost any transformation. *Physical Review Letters*, 80(19), 4329.
- [18] Grover, L. K. (1996, July). A fast quantum mechanical algorithm for database search. In Proceedings of the twenty-eighth annual ACM symposium on Theory of computing (pp. 212-219).
- [19] Brassard, G., Hoyer, P., Mosca, M., & Tapp, A. (2002). Quantum amplitude amplification and estimation. *Contemporary Mathematics*, 305, 53-74.
- [20] 15-qubit backend: IBM Q team, "IBM Q 16 Melbourne backend specification V2.1.0", (2020).  
Retrieved from <https://quantum-computing.ibm.com>
- [21] 5-qubit backend: IBM Q team, "IBM Q 5 Rome backend specification V1.0.0", (2020).  
Retrieved from <https://quantum-computing.ibm.com>
- [22] 5-qubit backend: IBM Q team, "IBM Q 5 London backend specification V1.0.0", (2020).  
Retrieved from <https://quantum-computing.ibm.com>
- [23] 5-qubit backend: IBM Q team, "IBM Q 5 Burlington backend specification V1.1.4", (2020).  
Retrieved from <https://quantum-computing.ibm.com>
- [24] 5-qubit backend: IBM Q team, "IBM Q 5 Essex backend specification V1.0.1", (2020).  
Retrieved from <https://quantum-computing.ibm.com>
- [25] 5-qubit backend: IBM Q team, "IBM Q 5 Ourense backend specification V1.0.1", (2020).  
Retrieved from <https://quantum-computing.ibm.com>
- [26] 5-qubit backend: IBM Q team, "IBM Q 5 Vigo backend specification V1.0.1", (2020).  
Retrieved from <https://quantum-computing.ibm.com>
- [27] 5-qubit backend: IBM Q team, "IBM Q 5 Armonk backend specification V1.1.0", (2020).  
Retrieved from <https://quantum-computing.ibm.com>

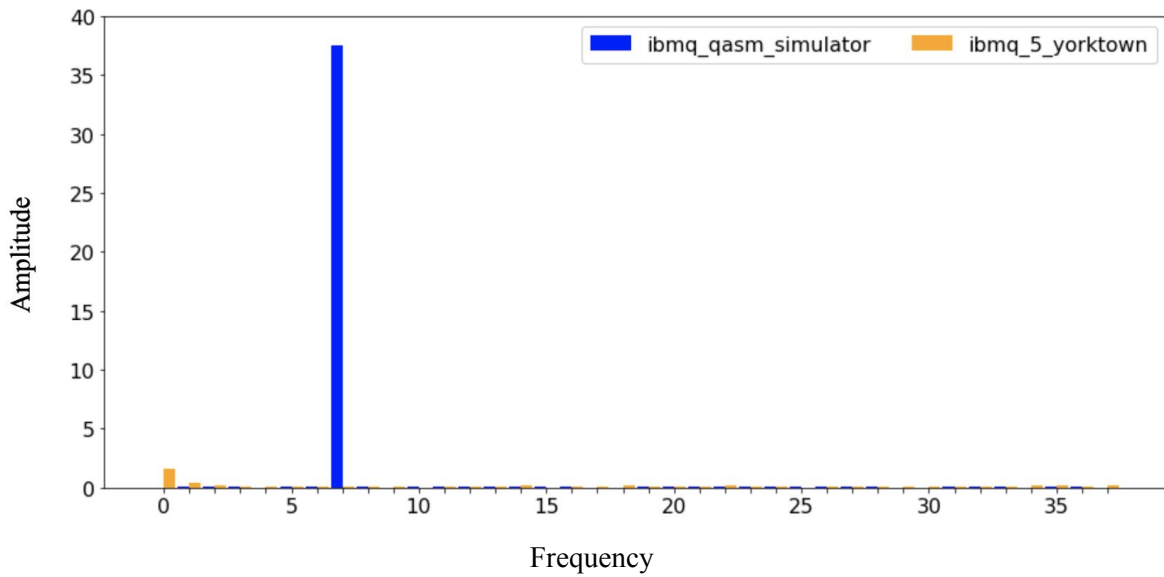
- [28] Nielsen, M. A., & Chuang, I. (2002). Quantum computation and quantum information.
- [29] Python, version 3.7.6.  
<https://www.python.org>
- [30] Jupyter, version 1.0.0.  
<https://jupyter.org>
- [31] Source code repository of the thesis  
<https://github.com/michaelnitsenko/thesis>
- [32] McKay, D. C., Alexander, T., Bello, L., Biercuk, M. J., Bishop, L., Chen, J., ... & Gomez, J. (2018). Qiskit backend specifications for OpenQASM and OpenPulse experiments. arXiv preprint arXiv:1809.03452.
- [33] Abraham Asfaw, Luciano Bello, Yael Ben-Haim, Sergey Bravyi, Lauren Capelluto et al. (2020). Learn Quantum Computation Using Qiskit.  
<http://community.qiskit.org/textbook>
- [34] SciPy, version 1.4.1  
<https://www.scipy.org>

# Appendix

## I. Figures and tables of the experiments excluded from section 3

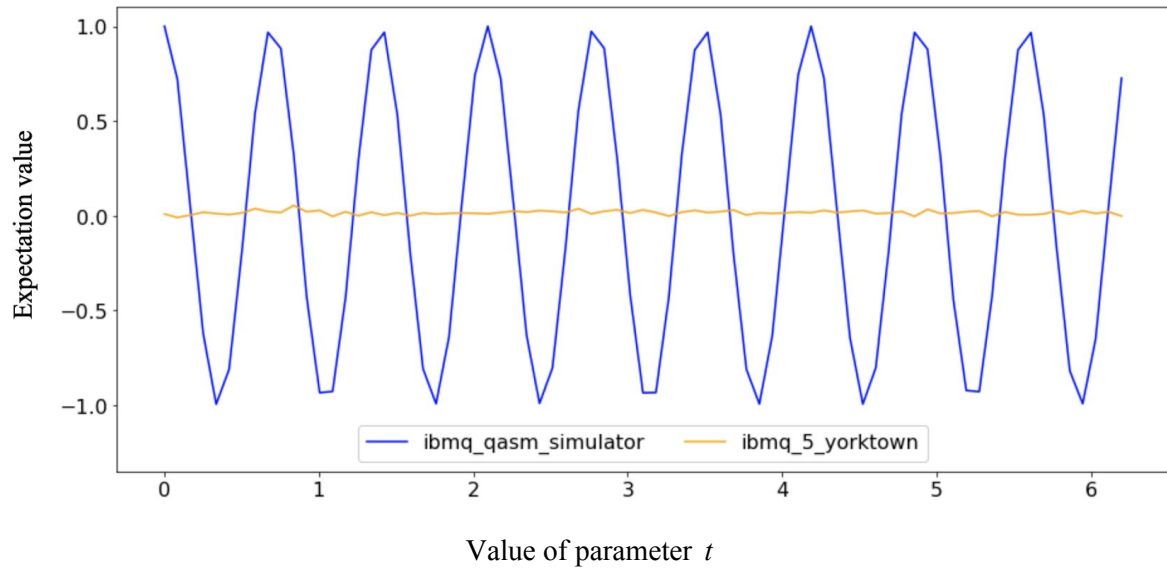


a

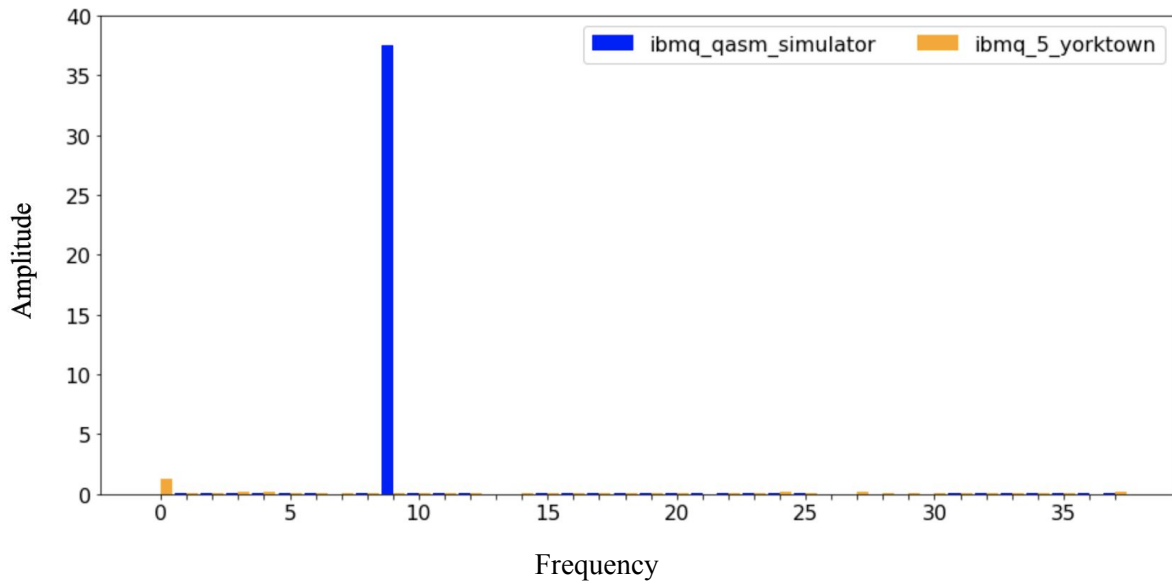


b

Fig. II.1 Expectation values (a) and Fourier analysis (b) of experiment (4;3)

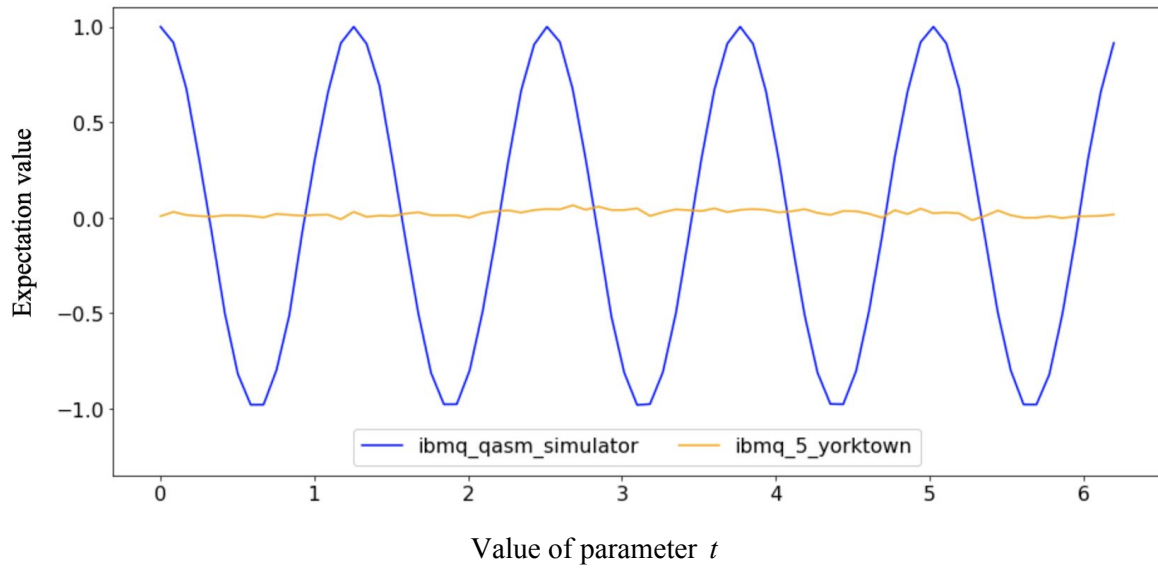


a

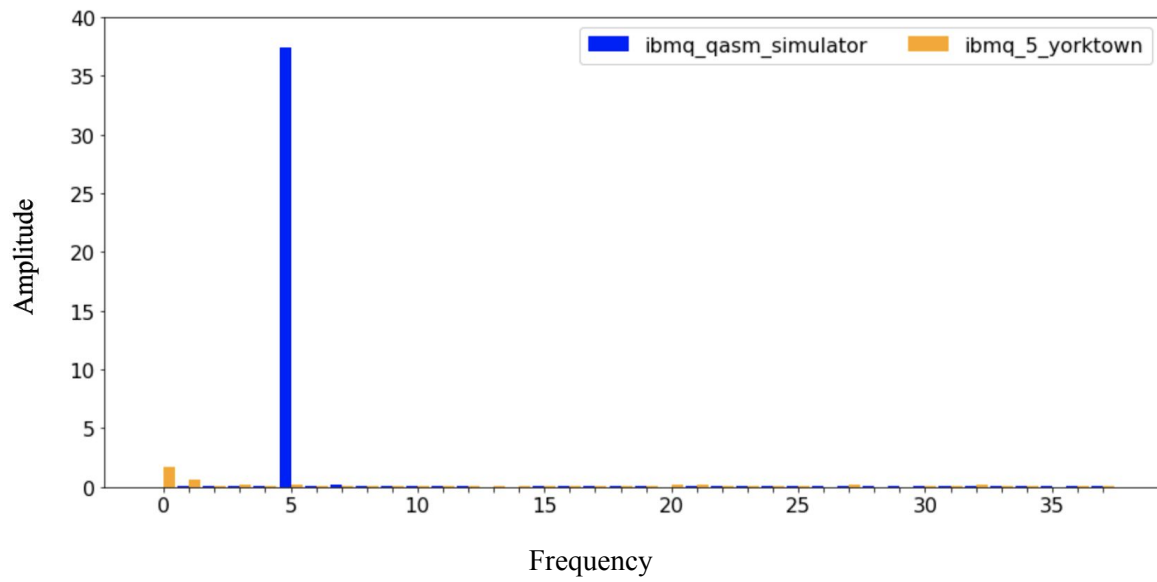


b

Fig. II.2 Expectation values (a) and Fourier analysis (b) of experiment (4;4)

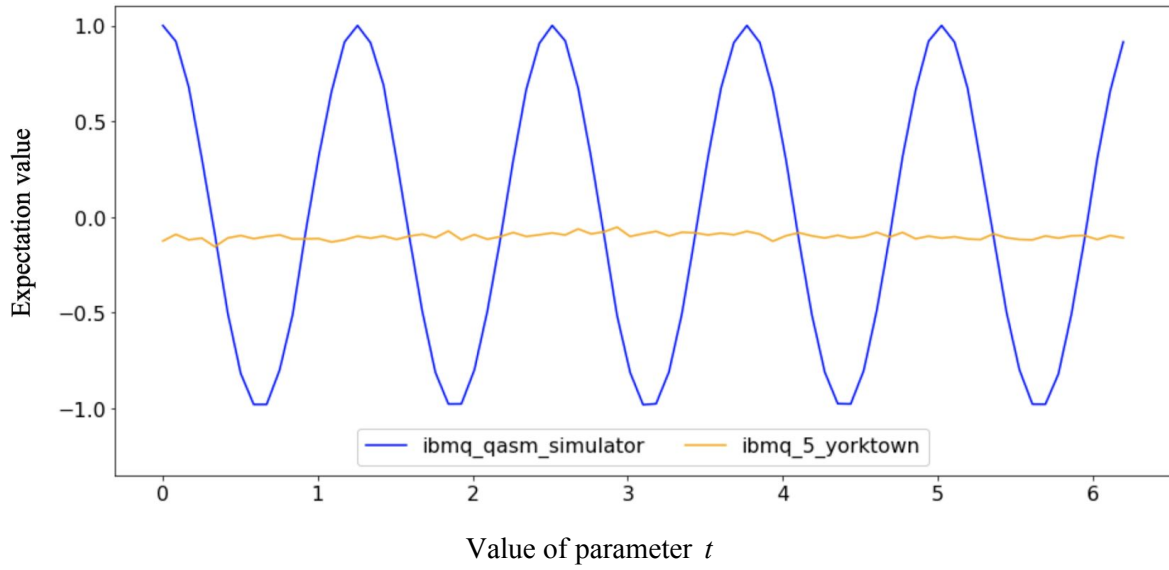


a

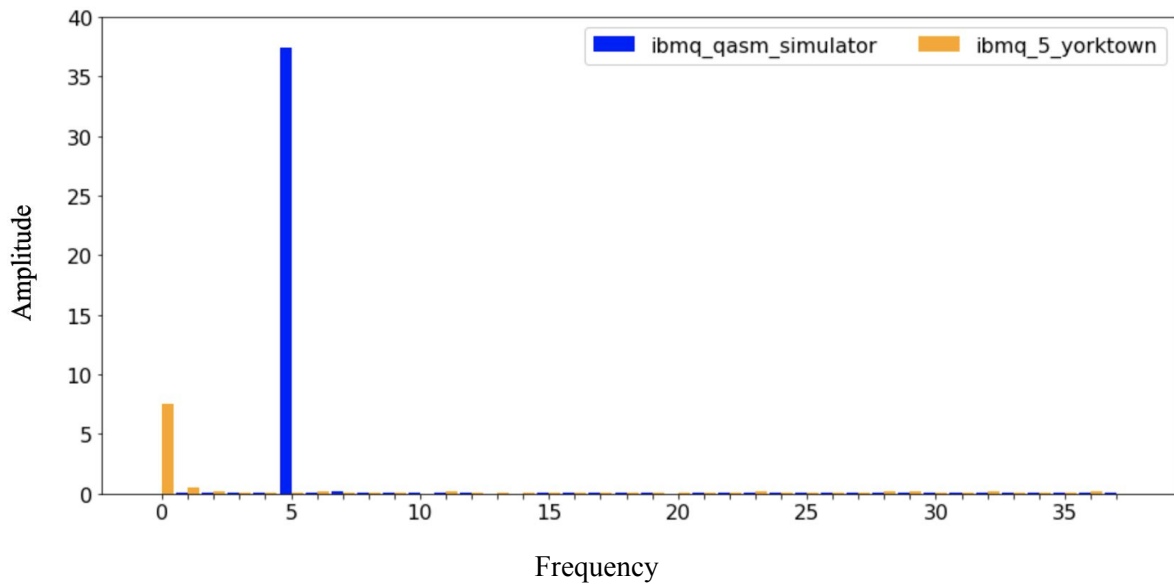


b

Fig. II.3 Expectation values (a) and Fourier analysis (b) of experiment (4;2)

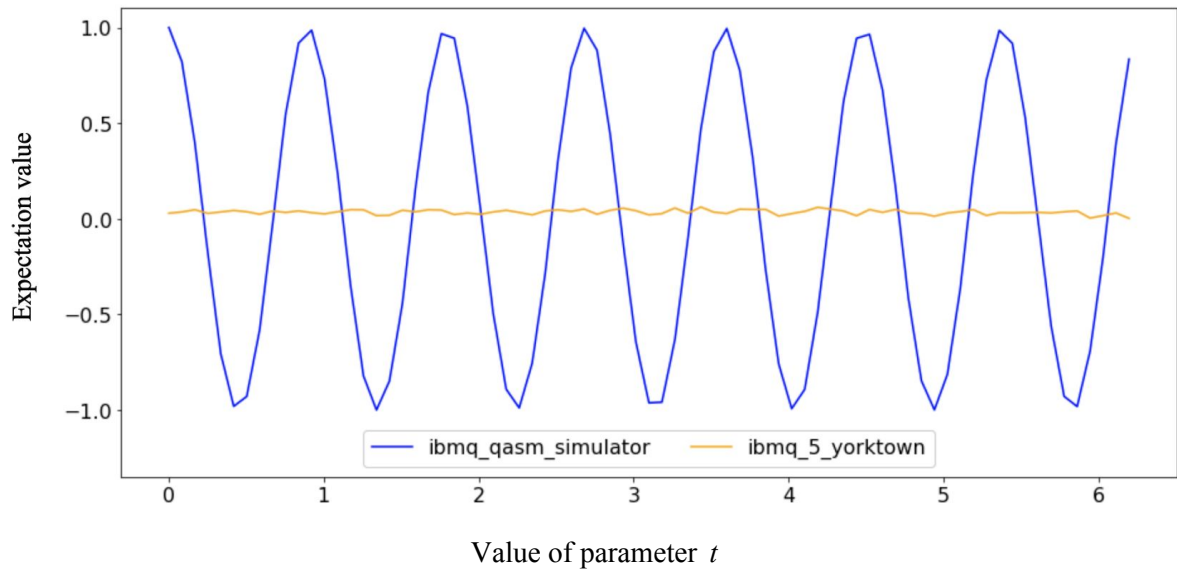


a

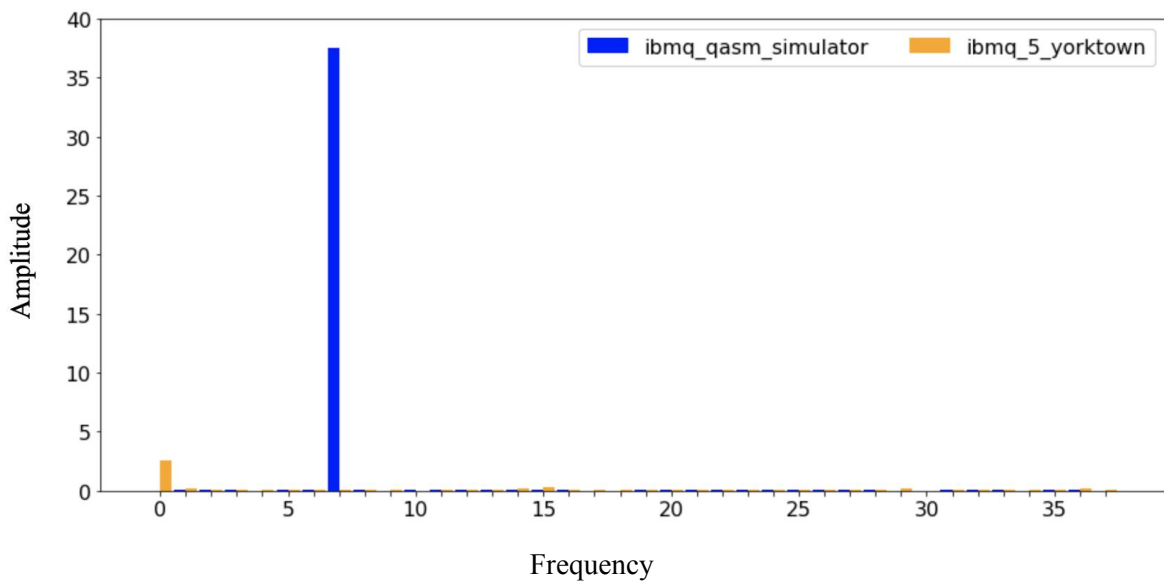


b

Fig. II.4 Expectation values (a) and Fourier analysis (b) of experiment (5;2)

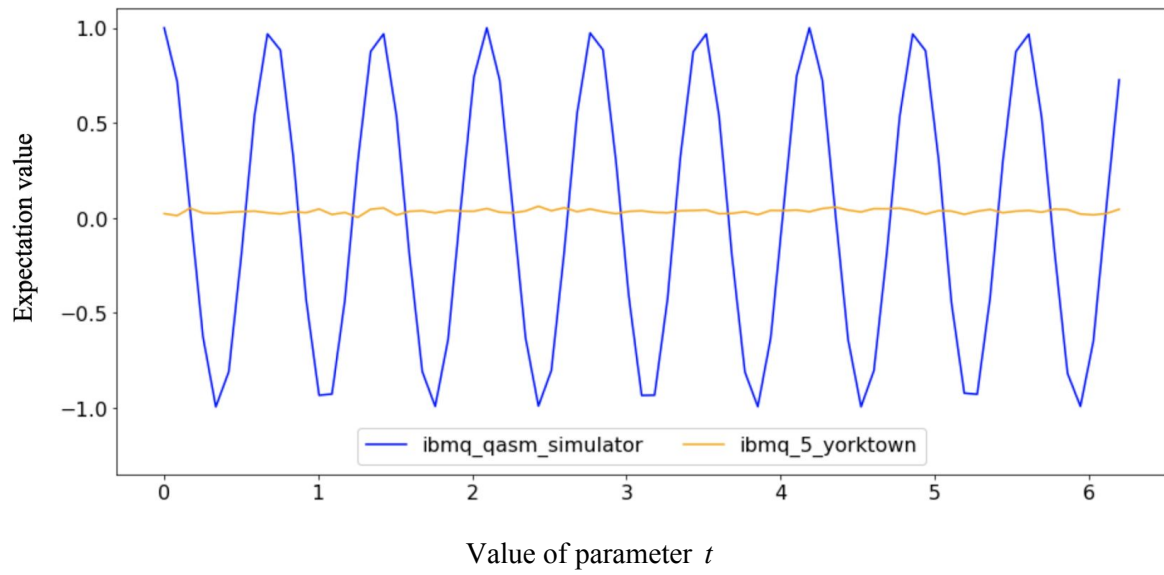


a

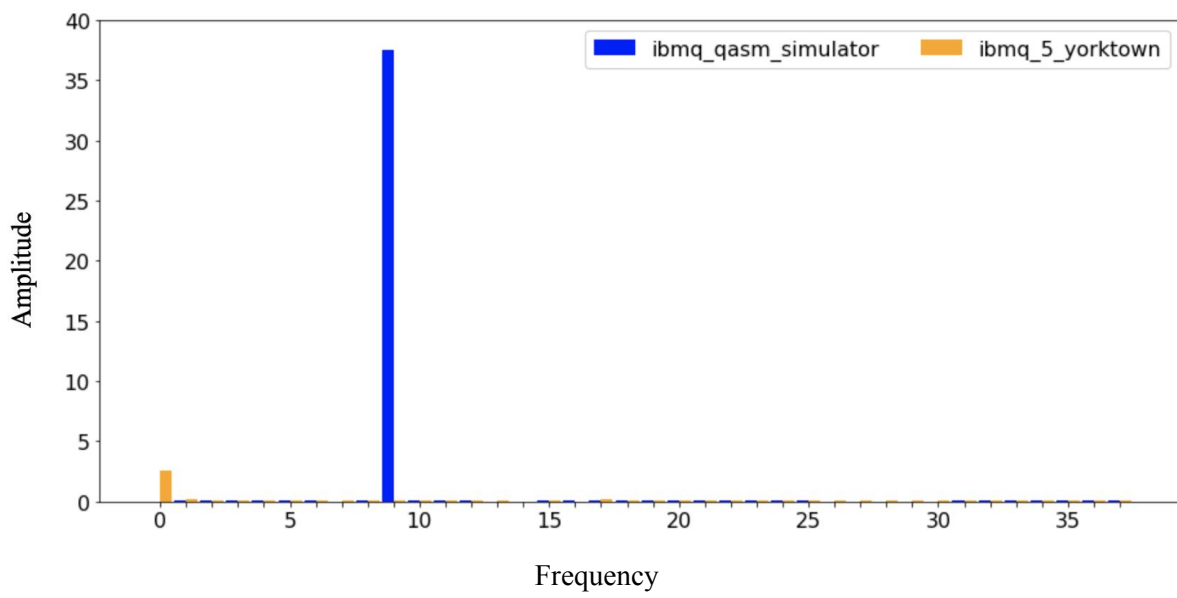


b

Fig. II.5 Expectation values (a) and Fourier analysis (b) of experiment (5;3)



a



b

Fig. II.6 Expectation values (a) and Fourier analysis (b) of experiment (5;4)

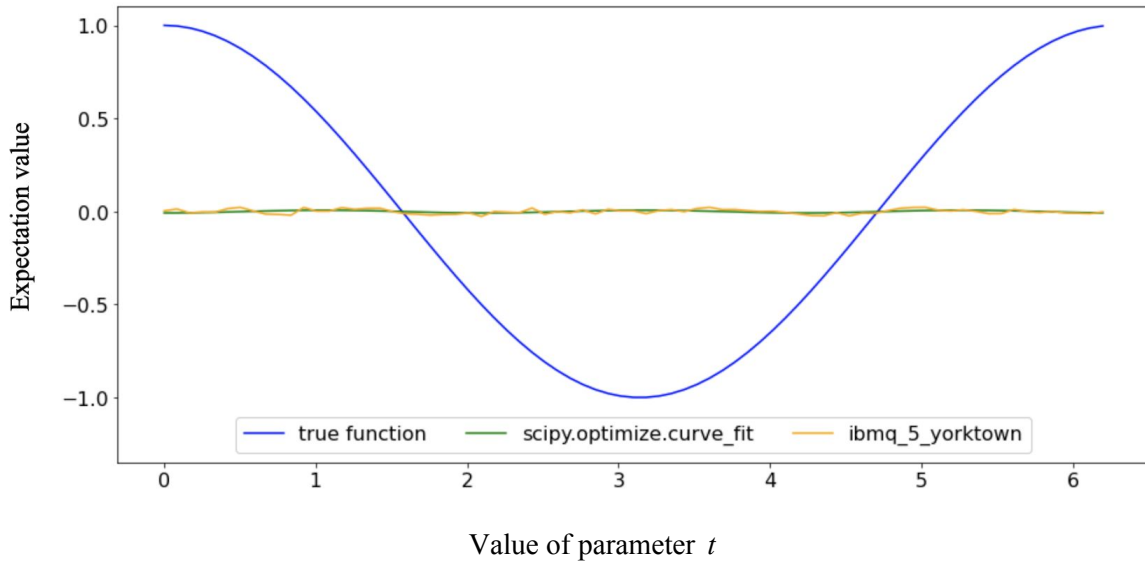


Fig. II.7 Expectation values of the  $m^3$  circuits fusion (3 qubit system), the function (3.2) with parameters fitted to the fusion curve (green) and the function (3.1) (blue)

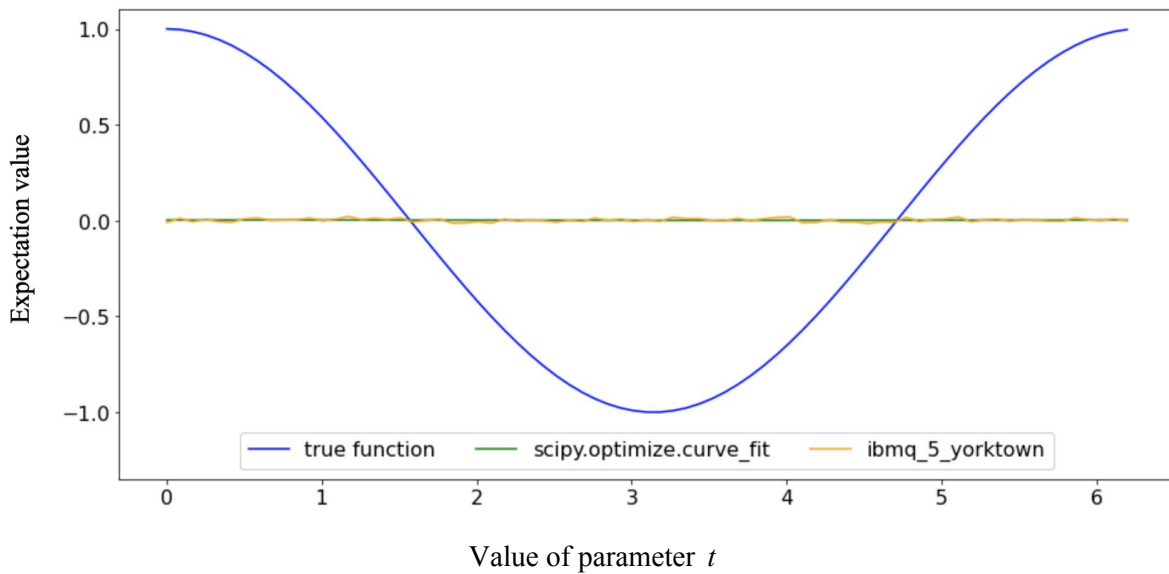


Fig. II.8 Expectation values of the  $m^4$  circuits fusion (3 qubit system), the function (3.2) with parameters fitted to the fusion curve (green) and the function (3.1) (blue)

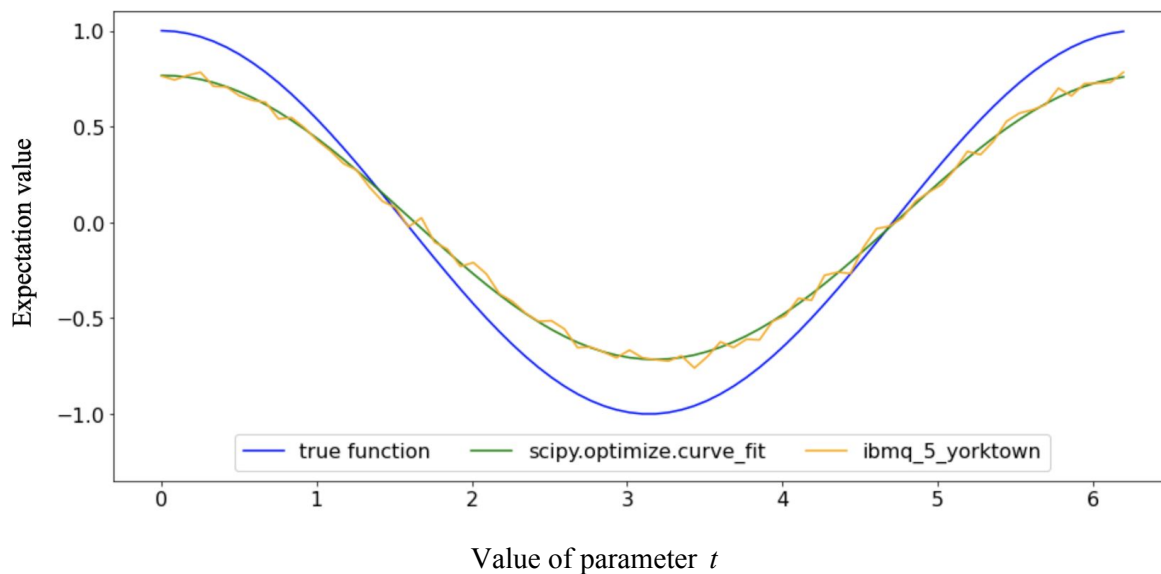


Fig. II.9 Expectation values of the  $m^0$  circuits fusion (5 qubit system), the function (3.2) with parameters fitted to the fusion curve (green) and the function (3.1) (blue)

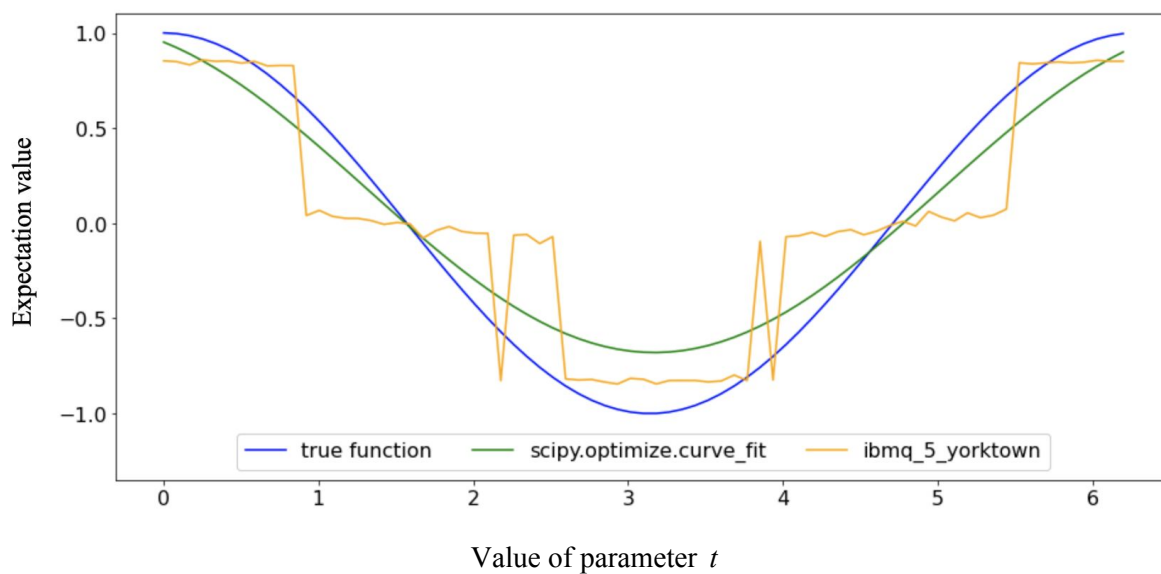


Fig. II.10 Expectation values of the  $m^1$  circuits fusion (5 qubit system), the function (3.2) with parameters fitted to the fusion curve (green) and the function (3.1) (blue)

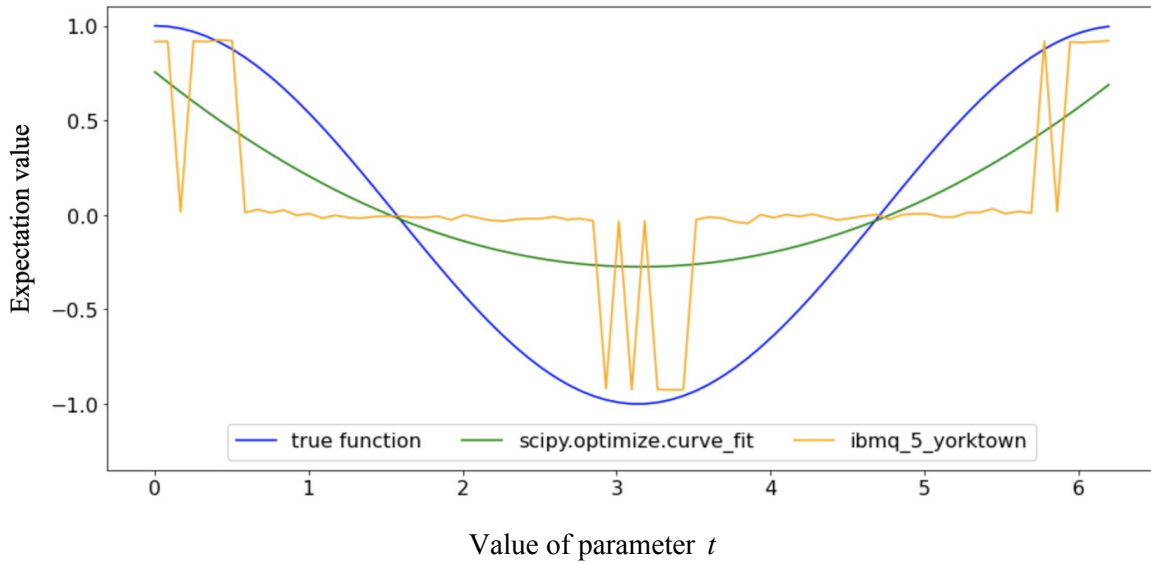


Fig. II.11 Expectation values of the  $m^2$  circuits fusion (5 qubit system), the function (3.2) with parameters fitted to the fusion curve (green) and the function (3.1) (blue)

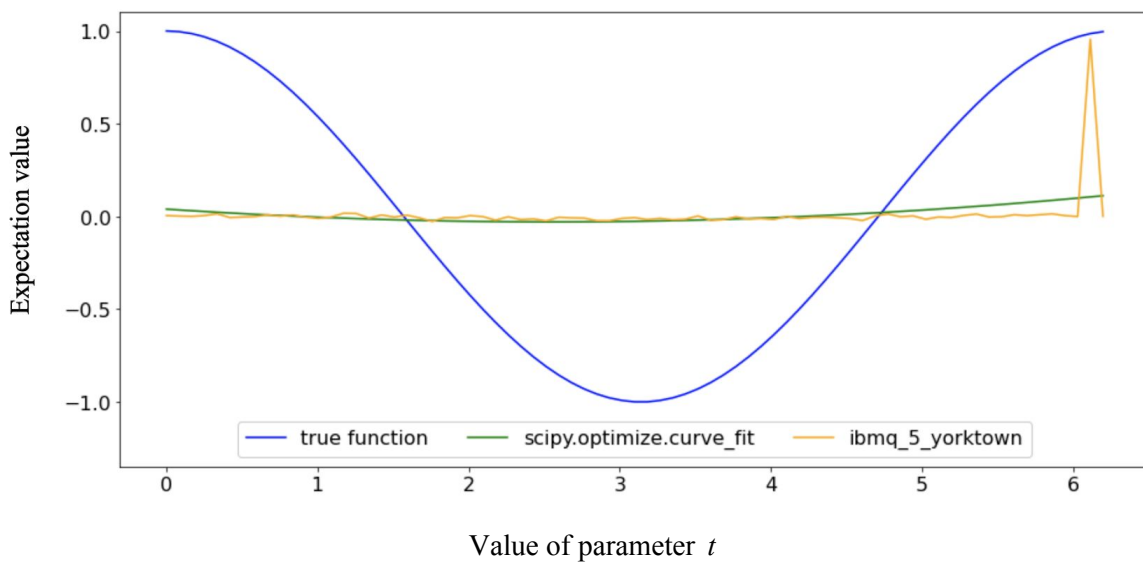


Fig. II.12 Expectation values of the  $m^3$  circuits fusion (5 qubit system), the function (3.2) with parameters fitted to the fusion curve (green) and the function (3.1) (blue)

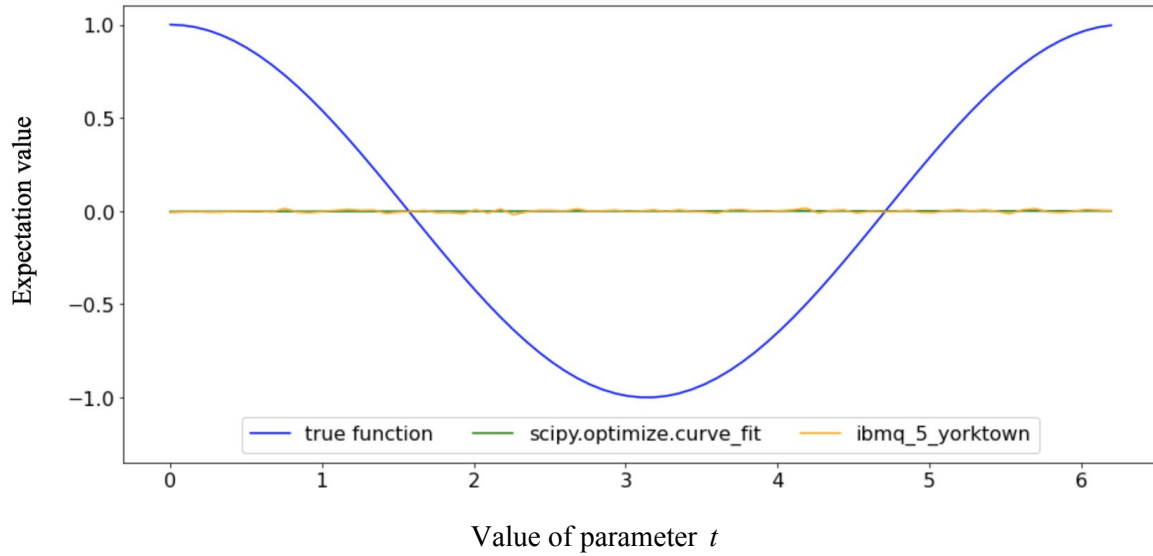


Fig. II.13 Expectation values of the  $m^4$  circuits fusion (5 qubit system), the function (3.2) with parameters fitted to the fusion curve (green) and the function (3.1) (blue)

Table II.1 Parameters of the expectation value function (3.2) fitted to the fusion of  $m^j$  circuits (5 qubit system)

$j$	$p_0$	$p_1$	$p_2$	$p_3$	MSE
0	0.99296	-0.01605	0.74088	0.02528	0.00079
1	0.84493	0.46207	0.86075	0.18139	0.05519
2	0.00952	3.11157	2286.91320	2286.63862	0.08272
3	-0.00806	3.16215	326.16926	326.14001	0.01081
4	0.01347	6.202332	1.14489	-1.14425	0.00004

# License

## Non-exclusive licence to reproduce thesis and make thesis public

I, Mykhailo Nitsenko,

1. herewith grant the University of Tartu a free permit (non-exclusive licence) to reproduce, for the purpose of preservation, including for adding to the DSpace digital archives until the expiry of the term of copyright,

### **Quantum circuit fusion in the presence of quantum noise on NISQ devices,**

supervised by Dirk Oliver Theis and Dominique Unruh.

2. I grant the University of Tartu a permit to make the work specified in p. 1 available to the public via the web environment of the University of Tartu, including via the DSpace digital archives, under the Creative Commons licence CC BY NC ND 3.0, which allows, by giving appropriate credit to the author, to reproduce, distribute the work and communicate it to the public, and prohibits the creation of derivative works and any commercial use of the work until the expiry of the term of copyright.
3. I am aware of the fact that the author retains the rights specified in p. 1 and 2.
4. I certify that granting the non-exclusive licence does not infringe other persons' intellectual property rights or rights arising from the personal data protection legislation.

*Mykhailo Nitsenko*

**15/05/2020**